

4

Basic concepts in ferromagnetism of diluted magnetic semiconductors. The case of manganese embedded in Ge(001)

George A. Lungu, Nicoleta G. Apostol, Cristian M. Teodorescu*

National Institute of Materials Physics, Atomistilor 105b, 077125 Magurele-Ilfov, Romania

*Corresponding author

Outline:

Introduction.....	75
Basic aspects.....	75
Exchange interaction. The Heisenberg model. Hysteresis.....	76
Basic theories of ferromagnetism for metals.....	82
Direct exchange.....	82
Band (Stoner) ferromagnetism.....	83
Zener model. Indirect exchange.....	85
A Stoner-Zener model.....	87
Superparamagnetism.....	88
Spin glasses.....	89
RKKY interaction.....	90
The s-d exchange integral.....	91
Perturbation theory.....	92
Computing the RKKY interaction. Orders of magnitude.....	94
Summary of exchange mechanisms and their fingerprints in M(H, T) behaviours.....	97
The case of manganese diluted into Ge(001)	98
Overview.....	98
Structure and morphology (LEED, HRTEM)	99
Composition (XPS)	100
Magnetic properties (SQUID)	101
Conclusions.....	105
Acknowledgements.....	106
References.....	107

Introduction

Diluted magnetic semiconductors (DMS) are materials extensively studied nowadays, owing to the fact that the magnetic order is intimately connected to the density of charge carriers in the semiconductor, hence offering new possibilities of magnetism control via the charge carriers. The basic mechanisms responsible for this indirect exchange are those developed five decades ago by Zener and by Ruderman-Kittel-Kasuya-Yosida. However, implementing these mechanisms in the practical analysis of magnetic properties, reflected in the evolution of magnetization with applied field and temperature $M(H, T)$ is still not standardized. The first part of this Chapter analyzes briefly all basic mechanisms which may lead to ferromagnetism, from direct exchange to indirect exchange, treating also the cases of spin glasses and superparamagnetic systems, which sometimes coexist with ferromagnetic phases. The second part of the Chapter applies the developed concepts to the case of a diluted magnetic semiconducting system quite studied during the last decade, the case of manganese embedded into germanium.

Ge(001) surfaces are relatively easy to be prepared, have a higher stability in ultrahigh vacuum as compared with Si(001), and are compatible with silicon-based technology. Therefore, magnetic systems synthesized on or inside Ge(001) may provide a valid alternative for integration of ferromagnetic functionalities onto semiconductor electronics.

Room temperature ferromagnetic Mn-Ge systems are obtained by simple deposition of manganese on Ge(001) heated at relatively high temperature (starting with 250 °C). The samples are characterized by low energy electron diffraction (LEED), high resolution transmission electron microscopy (HRTEM), X-ray photoelectron spectroscopy (XPS), magneto-optical Kerr effect (MOKE) and superconducting quantum interference device (SQUID) measurements. Samples deposited at relatively elevated temperature (350 °C) exhibited the formation of $\sim 5\text{-}8$ nm diameter Mn_5Ge_3 and $\text{Mn}_{11}\text{Ge}_8$ agglomerates by HRTEM, while XPS (Ge 3d, Ge 2p and Mn 2p) identified at least two Mn-containing phases: the agglomerates, together with a Ge-rich phase, or manganese diluted into the Ge(001) crystal. LEED revealed the persistence of long range order, including the $(2 \times 1) - (1 \times 2)$ Ge(001) reconstructions after a relatively high amount of Mn (100 nm) deposited on the single crystal substrate. The films exhibited a clear ferromagnetism at room temperature, while SQUID measurements as function on temperature revealed the co-existence of a ferromagnetic and of a superparamagnetic phase with RKKY interaction.

Basic aspects

The main characteristics of the ferromagnetism are the following:

- a) the presence of a hysteresis curve of the magnetization vs. the applied magnetic field $M(H)$, which automatically implies the existence of a 'remanent magnetization' M_r even in zero applied field, once the sample was magnetized, i.e. it experienced a higher applied field along one direction;
- b) the fact that the permanent magnetization (and implicitly the remanent magnetization) decrease with temperature. At temperatures above the Curie temperature T_c , no remanence may be obtained and the system behaves like a paramagnet, i.e. it exhibits a weak magnetization with the applied field;
- c) the second derivatives of the free energy with respect to temperature and to the applied field have discontinuities, therefore there is a phase transition at the Curie temperature between

the ferromagnetic and the paramagnetic state. The physical quantities exhibiting discontinuities are the specific heat and the magnetic susceptibility.

In the following, we shall concentrate mostly on the hysteresis curves and on their evolution with temperature, pointing out the main mechanisms responsible for ferromagnetism: direct exchange of insulated spins, band ferromagnetism of delocalized electrons, and indirect exchange mechanisms, which are of paramount importance for diluted magnetic semiconductors.

Exchange interaction. The Heisenberg model. Hysteresis

The Heisenberg model is derived from the energy separation between the triplet and the singlet states for a two-electron system $E_H = -2J \mathbf{S}_1 \cdot \mathbf{S}_2$, where J is the Heisenberg exchange interaction, and $\mathbf{S}_{1,2}$ are the spins of the two interacting electrons. For two electrons belonging to two neighboring atoms A and B described by the spatial wavefunctions $\Psi_{A,B}(\mathbf{r})$ with the radial origin being each atom, the exchange interaction is written as [1]:

$$J = e_0^2 \int d^3r_1 d^3r_2 \Psi_A^*(\mathbf{r}_1) \Psi_B^*(\mathbf{r}_2) \left\{ \frac{Z_A Z_B}{|\mathbf{R}_A - \mathbf{R}_B|} - \frac{Z_A}{|\mathbf{R}_A - \mathbf{r}_2|} - \frac{Z_B}{|\mathbf{R}_B - \mathbf{r}_1|} + \frac{1}{|\mathbf{r}_1 - \mathbf{r}_2|} \right\} \Psi_B(\mathbf{r}_1) \Psi_A(\mathbf{r}_2) \quad (1)$$

where $\Psi_{A,B}$ satisfy the one-electron Schrödinger equations for atoms A and B:

$$-\frac{\hbar^2}{2m} \Delta_1 \Psi_A(\mathbf{r}_1) - \frac{Z_A e_0^2}{|\mathbf{R}_A - \mathbf{r}_1|} \Psi_A(\mathbf{r}_1) = \varepsilon_A \Psi_A(\mathbf{r}_1) \quad (2a)$$

$$-\frac{\hbar^2}{2m} \Delta_1 \Psi_B(\mathbf{r}_2) - \frac{Z_B e_0^2}{|\mathbf{R}_B - \mathbf{r}_2|} \Psi_B(\mathbf{r}_2) = \varepsilon_B \Psi_B(\mathbf{r}_2) \quad (2b)$$

Z_A and Z_B are charges of ions A and B, $e_0^2 = e^2 / (4\pi\epsilon_0)$ the reduced square of the elementary charge. The Coulomb interaction K in the Heitler-London model is similar to eq. (1), but with indices A and B interverted in the last product of wavefunctions at the right-hand side, which separates the charge densities $\rho_{A,B} = |\Psi_{A,B}|^2$ in the integral, and give to the expression an immediate intuitive explanation: it is composed by the mutual repulsion between ions A and B, the attraction of the electron located on B by the ion A and that of the electron located on A by the ion B, plus the mutual repulsion of the two charge densities associated to both electrons. It will be somehow clear that the Coulomb interaction will decrease with increasing mutual separation between atoms A and B. The energies of the triplet (spins aligned, $\uparrow\uparrow$) and singlet ($\uparrow\downarrow$) states are given by $E_{S,T} = \varepsilon_A + \varepsilon_B + K \pm J$, therefore their separation is $2J$, with the triplet state being energetically more favorable for positive values of the exchange integral.

There is no intuitive view of the exchange interaction. It occurs owing to the indiscerability of both electrons. In the Heisenberg model, the interacting magnetic systems are composed by isolated ions with incomplete outer shells; on these shells, according to Hund's rules, individual electron spins are placed such as to maximize the overall projection on a chosen z axis (the axis corresponding to the eventual application of an external magnetic field). For example, a d^7 outer shell will exhibit a spin configuration such as $\uparrow\downarrow\uparrow\downarrow\uparrow\uparrow\uparrow$, with a net electronic magnetic moment along the z axis of 3 Bohr magnetons (μ_B). The Heisenberg model assumes that a similar inter-atomic or inter-ionic exchange is valid for the total (atomic or ionic) spin moments, $H_{\text{int., 12}} = -2 J_{12} \mathbf{S}_{1, \text{tot}} \cdot \mathbf{S}_{2, \text{tot}}$.

Mean field theory takes the average over all interacting spins (around, let's say, \mathbf{S}_i , centred on ion i), by replacing \mathbf{S}_j ($j \neq i$) with its average value $\langle \mathbf{S}_j \rangle$. This corresponds to the introduction of an internal ('molecular') field (in MKSA units):

$$\mathbf{H}_m = \frac{\sum_{j \neq i} J_{ij} \langle \mathbf{S}_j \rangle}{\mu_0 \mu_r \mu_B} \approx \frac{J \eta \langle \mathbf{S} \rangle}{\mu_0 \mu_r \mu_B} \approx \frac{J \eta \mathbf{M}}{2 n \mu_0 \mu_r \mu_B^2} \equiv \lambda \mathbf{M}; \quad \lambda_H = \frac{J \eta}{2 n \mu_0 \mu_r \mu_B^2} \quad (3)$$

where the gyromagnetic factor was considered 2, for simplicity; μ_0 is the permeability of vacuum, μ_r is the relativity permeability of the material, and the successive approximation point on the prevalence of a constant near-neighbor exchange interaction, with η near neighbors around each spin \mathbf{S}_i . n is the density of magnetic atoms or ions. Equation (3) introduces also the Weiss 'molecular field constant', λ_H , with the subscript "H" accounting for "Heisenberg".

The paramagnetism of bound electrons is obtained in the classical theory by averaging the projection of elemental magnetic moments μ_z ranging from $-\mu_{\max.}$ to $\mu_{\max.}$, with inclusion of the statistical term $\exp(\mu_z \mu_0 H / k_B T)$. The computation is straightforward, and the Langevin function $L(x) = \coth(x) - 1/x$ (with $x = \mu_{\max.} \mu_0 H / k_B T$) is obtained. In the quantum theory, the integral is replaced by a sum over all $(2S + 1)$ values of the spin projection over the axis of the applied magnetic field, and the Brillouin function is obtained (we will drop the vector notation for field and magnetization, assuming that these vectors are colinear):

$$M(H) = 2n\mu_B S \times B_S \left(\frac{2\mu_0 \mu_r \mu_B S H}{k_B T} \right) \quad (4)$$

with

$$B_S(y) = \frac{2S+1}{2S} \coth \left(\frac{2S+1}{2S} y \right) - \frac{1}{2S} \coth \frac{y}{2S} \approx \coth(y) - \frac{1}{y} \quad \text{for large values of } S \quad (5)$$

The need to introduce the relative permeability of the material μ_r will be justified later. The Langevin function is obtained as a limit of the Brillouin function when $S \rightarrow \infty$. The Weiss theory of ferromagnetism implies solving of an equation derived from (4):

$$M(H) = 2n\mu_B S B_S \left\{ \frac{2\mu_0 \mu_r \mu_B S}{k_B T} (H + \lambda M) \right\} \quad (6)$$

For high temperatures or low values of J or of λ , the above equation has only one solution, $M = 0$ for $H = 0$, $M \neq 0$ for $H \neq 0$. The system is in the paramagnetic state. For parameters yielding a stepped shape of the function B_S , equation (6) starts to have three solutions. Even for $H = 0$, there are two symmetric nonvanishing solutions $M = \pm M_r \neq 0$. Also, a solution with $M > 0$ exist sometimes for $H < 0$, and viceversa. Increasing further the absolute value of $H < 0$ implies that at a given point only the solution with $M < 0$ exist. This is the origin of the hysteresis cycle in ferromagnets. Plotting all three M solutions of the above equation vs. H yields an 'S-shaped' curve, with the inner part corresponding to solutions with negative susceptibility $\chi = \partial M / \partial H$. These solutions must be discarded from thermodynamic considerations (they correspond to unstable states), and therefore a sudden jump is executed by the system when the field exceeds H_c . Figure 4.1 presents an illustration of all the considerations above, by

solving $\mu = B_S(h + \alpha\mu)$, and working in reduced variables, such as $\alpha = S^2 J \eta / (k_B T)$, $h = 2 \mu_0 \mu_r \mu_B S H / (k_B T)$, $\mu = M / (2n \mu_B S)$.

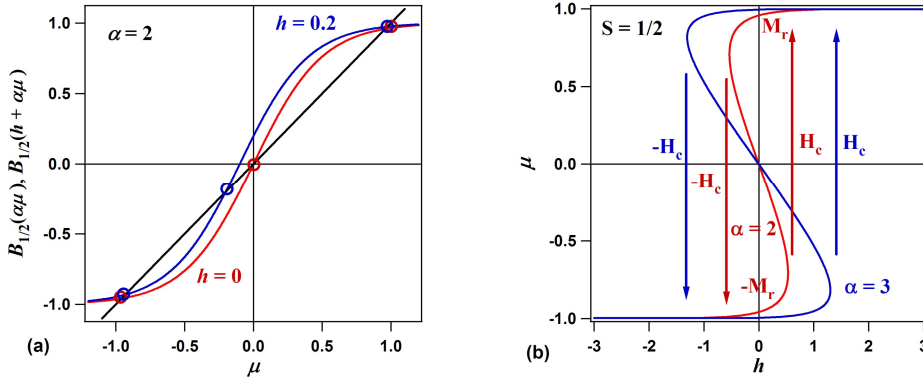


FIGURE 4.1

Examples of solutions for equation (6), translated here as $\mu = B_S(h + \alpha\mu)$. (a) represents the Brillouin function for $S = 1/2$, for zero (red curve) and nonzero (blue curve) applied field. Circles denote the three solutions. (b) represents the solutions found for two values of the interaction parameter (molecular field) α . A clear increase in the coercitive field is induced by larger α values

By setting $m = M/M_{\max}$ and $h = H/ M_{\max}$, and by using the Langevin function $L(x)$, the transcendent equation (6) may be written as $m = L(am + bh)$, which can be written as $bh = L^{-1}(m) - am$, with $M_{\max} = n \mu_{\max}$, $b = \mu_0 \mu_r n \mu_{\max}^2 / k_B T = \mu_0 \mu_r M_{\max} \mu_{\max} / k_B T$ and $a = b \lambda = J \eta / 2 k_B T$. As a general rule, in the following we will interpret the parameter a as the ratio between a characteristic microscopic energy ε_0 and the Boltzmann term $a = \varepsilon_0 / k_B T$, and the parameter b as the self-interaction of a magnetic moment μ_{\max} with the magnetic induction produced by these moments in the material. It is worth to be noted that $\mu_0 n \mu_B^2 \approx 6.755 \times 10^{-5}$ eV for usual atomic densities in solids $n = 10^{29} \text{ m}^{-3}$. In this case, the b parameter would be quite small at ‘usual’ temperatures $k_B T = 0.01\text{-}0.1$ eV, yielding the necessity of using elevated fields to produce noticeable modification of the magnetization curve, $H \approx 10^2 - 10^4 M_{\max}$. Thus, it is reasonable to introduce the relative permeability of the magnetic material in the above expressions, $\mu_r = 10^3 - 10^5$, yielding b values closer to unity.

By using $(\partial L / \partial x)_0 = 1/3$, it is clear that ferromagnetism occurs only if $a > 3$, therefore $a = 3T_c / T$. This immediately gives an order of magnitude for the energy ε_0 , it is of about 0.01-0.1 eV for most systems of interest. If the parameter b is on the order of unity, the molecular field constant λ yields as several units for ferromagnetic systems.

An approximation of the inverse of the Langevin function may be derived by taking into account that for small values of x , $L^{-1}(x) \approx 3x$, and for x close to ± 1 , $L^{-1}(x) \approx 1/(\pm 1 - x)$. In 1991, Cohen proposed the following approximate formula [2]:

$$L^{-1}(x) = \frac{3x - x^3}{1 - x^2} \tag{7}$$

Once again, the hysteresis curve can be described simply by $h(m) = \{L^{-1}(m) - am\} / b$. By setting $h = 0$, one obtains the remanent magnetization m_r ; by setting $\partial h / \partial m = 0$, one obtains the coercivity point m_c , then the coercitive field $h_c = h(m_c)$. As an exercise left to the reader, these values are derived as:

$$m_r = \pm \sqrt{\frac{a-3}{a-1}} \quad (8.1)$$

$$bh_c = \pm \sqrt{(a - \sqrt{4a-3})(a-1)} \frac{\sqrt{4a-3}-3}{\sqrt{4a-3}-1} \quad (8.2)$$

Let us stress that the important parameter for these reduced values is $a = b\lambda$. Another simple exercise is to replace in the above formulas $a = 3T_c/T$ and to derive that, in the neighborhood of the Curie temperature, the coercitive field behaves as $(1 - T/T_c)^{3/2}$ and the remanent magnetization as $(1 - T/T_c)^{1/2}$.

By using the inverse Langevin function, the transcendent equation $m = L(am + bh)$ may be transformed into an algebraic equation of third degree, whose solution for one branch of the magnetization curve $M(H)$ may be written as:

$$m = \frac{2\sqrt{3(a-1)(a-3) + (bh)^2}}{3(a-1)} \cos(h) \left\{ \frac{1}{3} \cos(h)^{-1} \frac{27bh(a-1)^2 - 2(bh)^3 - 9bh(a-1)(a-3)}{2[3(a-1)(a-3) + (bh)^2]^{3/2}} \right\} - \frac{bh}{3(a-1)} \quad (9)$$

where the \cos and \cos^{-1} function are to be considered when the argument is real and lower than 1 in absolute value, otherwise the corresponding hyperbolic functions \cosh and \cosh^{-1} are employed. When the argument is imaginary, \cosh is replaced by \sinh and \cosh^{-1} by \sinh^{-1} , and the square root at the denominator is taken from the absolute value. When the argument is real and lower than -1, \cosh^{-1} is taken from its absolute value and the overall sign is changed; this corresponds to the other branch of the hysteresis loop. When dealing with \cos^{-1} functions, in some cases different roots are to be considered, and phases $\pm 2\pi/3$ have to be added into the curly brackets.

An alternative explanation of the occurrence of magnetic hysteresis curves is the Stoner-Wohlfarth model of single domain ferromagnets [3], where the domains are supposed to exhibit, in absence of applied fields, a saturation magnetization M_s oriented along their easy magnetic axis. Applying a field along some angle (θ) with respect to the easy axis induces progressively the rotation of the magnetization in the direction of the applied field. If ϕ is the angle between the magnetization and the applied field, the magnetic energy per unit volume is written as:

$$\Delta E = K_u \sin^2(\theta - \phi) - \mu_0 H M_s \cos \phi \quad (10)$$

where K_u is the uniaxial anisotropy constant, and the second term is just the Zeeman energy. The equilibrium angle is found by minimizing equation (10):

$$H = \frac{K_u}{\mu_0 \mu_r M_s} \times \frac{\sin(2(\phi - \theta))}{\sin \phi} \quad (11)$$

The magnetization along the direction of the applied field is $M = M_s \cos \phi$. This equation, together with (11), define the $M(H)$ curve, with two branches, which can be written as:

$$H = \pm \frac{K_u}{\mu_0 \mu_r M_s} \times \left\{ \frac{2m^2 - 1}{\sqrt{1 - m^2}} \sin(2\theta) - 2m \cos(2\theta) \right\} \quad (12)$$

with $m = M/M_s$. The energy profiles allow one to derive the way the system evolves, with jumps from a branch to another, as represented in Figure 4.2. More rectangular hysteresis loops will be obtained when the angle between the applied field and the easy axis approaches zero. The coercive field may be computed from equation (11) by setting $\partial H/\partial m = 0$, and the remanent magnetization is computed by setting $H = 0$.

For random orientations of the applied field with respect to the easy axis, an immediate average of equation (12) for $0 \leq \theta \leq 90^\circ$ yields:

$$\langle h \rangle = \pm \frac{2}{\pi} \times \frac{K_u}{\mu_0 \mu_r M_s} \times \frac{2m^2 - 1}{\sqrt{1 - m^2}} \tag{13}$$

From here, the computation of the coercive field and of the remanent magnetization is straightforward, $M_r = M_s/2^{1/2}$ and $H_c = 2K_u/(\pi\mu_0 M_s)$.

One may see that the Weiss and the Stoner-Wohlfarth models are completely different approaches to explain the hysteresis curves. The Weiss molecular field approach works with the magnitude of the magnetization along the applied field, whereas the Stoner-Wohlfarth model supposes that a maximum magnetization is realized along the easy axis of the micromagnet and the magnetization just rotates in the applied field. Moreover, in the limiting case of applied field along the easy axis, the Weiss theory supposes a microscopic energy for each moment whose projection along the z axis is $2S\mu_B m$ as $\varepsilon_W = -2S\mu_0 H \mu_B m - 4S^2 \mu_0 \mu_B^2 n \lambda \langle m \rangle m$, whereas the Stoner-Wohlfarth energy may be written as $\varepsilon_{SW} = -2S\mu_0 H \mu_B m - \varepsilon_u m^2$, where $\varepsilon_u = K_u/n$ is the microscopic anisotropy energy. The main difference between these theories is that the Weiss model refers to a statistical ensemble of interacting spins, each one interacting with the external field and with the molecular field (already computed as an average of all spin projections) altogether, whereas the Stoner-Wohlfarth model analyses the behaviour of only one single domain system, but with uniaxial anisotropy. The statistical average for $H = 0$ in the latter case $\langle m \rangle = \int m x \exp(\varepsilon_{SW}/k_B T) dm / \int \exp(\varepsilon_{SW}/k_B T) dm$ vanishes when the average is performed for all m values ranging from -1 to $+1$, and for $H \neq 0$ just a paramagnetic behavior is obtained. However, for low temperatures $k_B T \ll \varepsilon_u$ and if the system was set in a well-defined state, e.g. $m = +1$, it is hard to believe that it will move spontaneously in a state with $m < 0$, therefore only values with $m = 1 - \delta m$, with $\delta m \ll 1$ should be considered in the average. This system is called in ‘frozen’ state. By waiting an infinite time, fluctuations would eventually lead to the realization of the state with opposite magnetic momentum $m = -1$. These concepts will be useful when we shall discuss superparamagnetism, in the next paragraph.

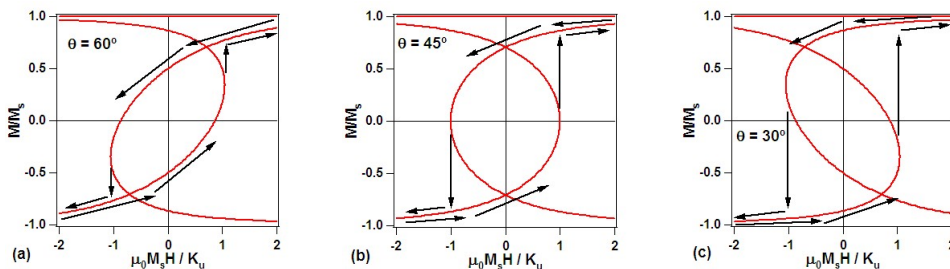


FIGURE 4.2 Examples of derivation of $M(H)$ curves from the Stoner-Wohlfarth theory, for three angles between the applied magnetic field and the easy magnetization axis

By setting in the expressions of the Weiss or of the Stoner-Wohlfarth energies $m = \langle m \rangle + \delta m$, it is easy to see that the two expressions become equivalent if $\delta m \ll \langle m \rangle$. Moreover, if $\varepsilon_{\text{SW}}(m)$ has two minima and the system has been prepared in one of them, if the barrier between minima exceeds the thermal energy, it is hard to believe that the system could overcome this barrier. Therefore, the system may be treated as exhibiting a single minimum, and the Weiss theory is applicable around this minimum. From the comparison between the Weiss and the approximation obtained for the Stoner-Wohlfarth energy, one may infer the molecular field constant in this case:

$$\lambda_{\text{SW}} = \frac{\varepsilon_u}{2nS^2\mu_0\mu_r\mu_B^2} \quad (14)$$

An unified theory was sketched by Callen, Liu, and Cullien [4]. Working in straightforward reduced variables (from equation (10)) and introducing an additional molecular field constant λ_0 , the magnetic energy is expressed as:

$$w = \frac{\Delta E}{K_u} = \sin^2(\theta - \phi) - (h + \lambda_0 \langle \cos \phi \rangle) \cos \phi \quad (15)$$

All consideration sketched previously are valid, but applied to the 'effective' field $h' = h + \lambda_0 m$. In particular, when $\theta = 90^\circ$, and, according to equation (12), the hysteresis area is expected to vanish, it may be seen that for $\lambda_0 > 2$ the hysteresis is again realized. Figure 4.3 represents the influence of including the molecular field constant in the case of a polycrystalline sample, where the angle averaging yielding to equation (13) is operated. It is clear that the presence of the molecular field constant fosters the ferromagnetism and enhances the area of the hysteresis curve. It may be demonstrated that in this case $\lambda_{\text{CLC}} = \lambda_0 + \lambda_u$.

The temperature dependencies in the Callen-Liu-Cullien model is obtained by averaging $\langle \cos \phi \rangle$, by integrating over all possible angles (from 0 to 360°) between the direction of the magnetization with respect to the applied field, and using the statistical factor $\exp(-\Delta E/nk_B T)$. At the end, a transcendent equation is obtained for $\langle \cos \phi \rangle$, as in the Weiss theory.

In the following, for simplification, each time we shall encounter in the energies a negative quadratic term in a parameter proportional to the magnetization, we shall treat it as a sign of ferromagnetism occurrence. This should be interpreted either in the framework of the Weiss model, with the statistical average implicitly understood in the computation of the average (Const. $\times \langle m \rangle m$) or in the framework of the Stoner-Wohlfarth model, by using a term such as Const. $\times m^2$, and by taking into account that, during the observation time, the system doesn't have the time to shift from $m > 0$ to $m < 0$ or viceversa.

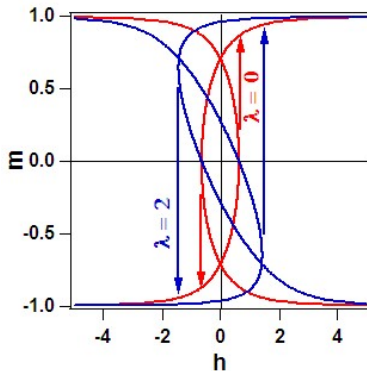


FIGURE 4.3

$m(h)$ curves obtained in the Stoner-Wohlfarth model, starting with the angle-averaged formula (12), and the effect of including a molecular field constant, as assumed by the Callen-Liu-Cullien model

Basic theories of ferromagnetism for metals

Despite the knowledge of ferromagnetism from the dawn of humanity, its origins in quite simple systems, such as ferromagnetic metals, is still subject to debates nowadays. It is hard to imagine our everyday life without magnetism, since they are used in all electrical motors, most of switches, recording media, etc. These magnets for practical use are most of them metallic. However, even for the explanation of ferromagnetism in simple transition metals (Fe, Co and Ni), three models have been developed so far: direct exchange, band ferromagnetism and the indirect exchange (Zener model). For more complicated systems, implying the dilution of magnetic ions in nonmagnetic matrices or the realization of magnetic clusters, other phenomena manifest, e.g. spin glasses or superparamagnetism. These phenomena will be treated at a very basic level in this paragraph, with the aim of outlining the main parameters which might be responsible for ferromagnetism.

a) Direct exchange

Early theories started by attributing ferromagnetism to direct exchange interaction between neighboring spins, much as in the case of the ferromagnetism of localized electrons. The first goal of any theory is to explain why ferromagnetism occurs in some metals only (at least, at room temperature). Everything starts with an eventual dependence of the exchange integral with the interatomic distance. A well-known plot for 3d transition metals (“the Bethe-Slater curve”) represents the exchange integral J as being small and positive for large values of the interatomic distance, increasing when the distance is reduced, reaching a maximum, then dropping to negative values when the interatomic distance (divided by the “typical dimension” of the 3d state) is lower than a critical value [5]. Fe, Co and Ni cases are placed on the positive branch of J , Mn and other transition metals with lower Z are placed on the negative branch. Despite criticism connected to the evaluation of Heitler-London integrals [6], the Bethe-Slater curve is still taught in most courses on magnetism and its behavior is often left as sole explanation for magnetism occurring only in the upper right corner of transition metals.

It is clear that the exchange integral will depend on the interatomic distance, the question is whether it may change its sign or not. A simple evaluation may be done starting with equation (1). The first term yields the factor $e_0^2 Z_A Z_B / R_{AB}$ multiplying $|S_{AB}|^2$, where the ‘superposition integral’ is given by $S_{AB} =$

$\int d^3r \Psi_A^*(r) \Psi_B(r)$. Now, for all r^{-1} -like denominators in the last three terms of equation (1), the leading contribution will be given by a volume δ^3 around ($r_2 \approx \mathbf{R}_A$) for the first term, around ($r_1 \approx \mathbf{R}_B$) for the second term, and around ($r_2 \approx r_1$) for the third term. Applying a 3-D mean value theorem for $Z_A = Z_B = Z$, this yields:

$$\frac{J}{e_0^2} = \frac{Z^2 |S_{AB}|^2}{R_{AB}} - 2Z\delta^2 \operatorname{Re}\{S_{AB} \Psi_A(\mathbf{R}_A) \Psi_B^*(\mathbf{R}_A)\} + \delta^2 \int d^3r |\Psi_A(r)|^2 |\Psi_B(r)|^2 \quad (16)$$

The second term vanishes for d states, since $\Psi_A(r) \sim |\mathbf{r} - \mathbf{R}_A|^{-2}$ (the hydrogen atom radial wavefunction corresponding to angular momentum l behaves as r^l). Therefore, equation (16) is expressed as a sum of two positively definite terms. A change of sign is expected only when the superposition of the d states is so large that for each of the second and the third terms of equation (1), important contributions to the integral will be given also by regions apart from the singularities ($r_2 \approx \mathbf{R}_A$) or ($r_1 \approx \mathbf{R}_B$).

Note also that modern computations confirmed partially the Bethe-Slater curve [7], however, for one-dimensional chains of transition metal atoms (from vanadium to cobalt).

b) Band (Stoner) ferromagnetism

The band theory of magnetism proposes a completely different approach. Here the electrons are delocalized over the whole crystal. It is assumed that the intrasite Coulomb repulsion favors the apparition of an asymmetry between the two subbands with opposite spins. The simplest model to account for the intrasite Coulomb repulsion is the Hubbard model, where, in second quantization, the Hamiltonian is written as [8,9]:

$$\hat{H} = T \sum_{\langle ij \rangle, \sigma} \hat{c}_i^{\sigma\dagger} \hat{c}_j^{\sigma} + U \sum_i \hat{n}_i^{\uparrow} \hat{n}_i^{\downarrow} \quad (17)$$

where σ stands for projection of spins on the z axis (\uparrow or \downarrow), $\langle ij \rangle$ means that the sum over j is performed on nearest neighbors of i only, such that the first term (the 'kinetic' one) represents the hopping of electrons with spin σ , and the second is the intrasite repulsion of electrons with opposite spin. There is an implicate assumption of this model, namely that it refers to a system of atoms where a maximum of two states with opposite spins may be accommodated on each site. However, it is often extrapolated to the practical case of magnetic metals, particularly to 3d transition metals [9-11]. An important observation we will point out is that, at equilibrium and for thermal energies $k_B T$ much lower than the Hubbard parameter U (which is of several eV), the intrasite Coulomb repulsion will prevent the placement of more than one electron on one site if the total number of electrons is less than half of the number of available sites. Therefore, the interacting term in this case will vanish, since the occupancy of each site i will be either \uparrow or \downarrow , randomly. Extrapolating to transition metals, this means that no Hubbard interaction is expected for metals whose available number of d electrons is lower than (or equal to) 5. Indeed, these metals (Sc, Ti, V, Cr, Y, Zr, Nb, Mo) hardly show ferromagnetism. A weak chromium ferromagnetism was detected at very low temperature in Refs. [12,13], and ferromagnetism of vanadium was measured in vanadium nanoparticles in Ref. [14]. It is to be expected that constraints, anisotropy and low dimensionality plays a vital role in stabilizing this ferromagnetism [9,10].

With this observation, for metals showing more than half of band occupancy, in average, the intrasite Coulomb repulsion from equation (16), when averaged on the vacuum state [9], yields the product of spin up and spin down electron densities. By introducing the asymmetry ξ , such that $n_{\uparrow, \downarrow} = n(1 \pm \xi)/2$,

the Coulomb interaction yields (per unit volume) $nU(1 - \xi^2)/4$. By discarding the unity term, which does not depend on the spin polarization, one obtains a quadratic decrease of the total energy (for given n larger than half of the available sites) as function on the asymmetry parameter. Therefore, the Hubbard interaction tends to induce a different occupancy of the \uparrow and \downarrow subbands. In the following, the subband with spin oriented \uparrow will be denoted as the 'majority' spin, and the band with spin \downarrow will represent the 'minority spin' subband. The next approximation is to suppose that the bands are splitted by the energy $\Delta\varepsilon$, i.e. the majority subband is shifted towards lower energies by $\Delta\varepsilon/2$, and the minority subband is shifted towards higher energies by the same amount. In fact, this is not true for densities of states $g(\varepsilon)$ varying strongly near the Fermi energy: for a more detailed analysis, the reader is invited to consult Refs. [9-11].

This asymmetry is accompanied by an increase of the average kinetic energy. For low asymmetry parameters ξ and not so stepped density of states, the kinetic energy increase of each electron is approximately $\Delta\varepsilon/2$, and there will be $n\xi/2$ electrons per unit volume participating to this kinetic energy increase. The asymmetry may be expressed as the integral of the density of states near the Fermi energy, over a range equal to the band splitting, and it may be approximated as $\xi \approx g(\varepsilon_F) \Delta\varepsilon$, with the density of states defined per electron. Therefore, the kinetic energy increase yields $(n\xi/2) \times (\Delta\varepsilon/2) \approx n\xi^2/[4g(\varepsilon_F)]$. Replacing this together with the energy decrease due to the Coulomb intrasite repulsion yields the energy difference per unit volume:

$$\Delta E_{ferro.} = \frac{n\xi^2}{4} \left(\frac{1}{g(\varepsilon_F)} - U \right) \quad (18)$$

From here, the Stoner criterion for ferromagnetism is straightforward, $Ug(\varepsilon_F) > 1$ [15]. Narrow bands, large intrasite repulsions and near half filling are needed for collective ferromagnetism.

Enough arguments may be formulated concerning both the Hubbard energy and the kinetic energy increase, for substituting ξ^2 with $\xi \langle \xi \rangle$ in (18) to yield a Weiss-like theory.

The molecular field constant can be easily derived in this case by assuming that the energy per unit volume may be written as magnetic interaction energy between the magnetization $M = n\xi\mu_B$ and the induction of the molecular field constant, such as $\Delta E_{ferro.} = -\mu_0\mu_r\lambda M^2$. The 'Stoner' molecular field constant follows:

$$\lambda_s = \frac{1}{4n\mu_0\mu_r\mu_B^2} \left(U - \frac{1}{g(\varepsilon_F)} \right) \quad (19)$$

which compares well with equation (3), for localized moments. It is clear that λ will increase if the intrasite Coulomb repulsion or the density of states at the Fermi level increases, it will also increase by decreasing the density of electrons. Nevertheless, one has to pay attention to this aspects, since the density of conduction electrons cannot be decreased to a value lower than half of the available sites, otherwise, as discussed previously, the Hubbard model cannot be applied. Therefore, the strongest magnetism occurs in metals with nearly half filled shells, but exceeding the half filling. This is the case of Fe of 3d elements, and of Ru of 4d elements. Indeed, more sophisticated calculations predicted the occurrence of band ferromagnetism in ruthenium [16].

Up to now, ferromagnetism appears to be a delicated balance between the Coulomb repulsion and attraction of each electron by the neighbouring atom, yielding the sign of J in the model of localized moments, or to a balance between the Coulomb intrasite repulsion energy and the inverse of the one-electron density of states, in the band model. The molecular field constant exceeds unity for typical

energies (the product $J\eta$, or half of the paranthesis in equation (18)) of 0.1-1 eV, and for relative permeability $\mu_r \sim 1000$. Also, increasing n , the density of interacting spins (in the localized model) or of conduction electrons yields to the decrease of the molecular field constant.

c) Zener model. Indirect exchange

The Zener model of exchange between localized moments and delocalized electrons [17] is another approach, which mixes ferromagnetism of localized electrons with that of delocalized ones. Zener pointed out that the Bethe-Slater curve might not be an accurate description of the direct exchange between atoms with d electrons and proposed that, no matter which is the interatomic separation distance, the direct exchange interaction is antiferromagnetic. He retained from the Bethe-Slater model the fact that the d electrons are localized on atomic centres and that they form a many-electron state which maximizes the projection of the total spin momentum (Hund's rule). In order to support the assertion that near-neighbor exchange must be antiferromagnetic, Slater analyzed the crystal structures of these materials and found out that, even for nonmagnetic metals, such as Ti, V, Cr, Zr, Nb, Mo, with d occupancies ranging from d^3 to d^5 (one supposes that one electron from the conduction band is left in the s state), the most stable structure is the body centred cubic (*bcc*) one, which can accomodate antiferromagnetic coupling with no frustration. Although more closely packed, the face centred cubic (*fcc*) and hexagonal close packed (*hcp*) structures are not realized (or are realized only in some particular cases) for those metals which are expected to exhibit a large value of the overall spin moment. (Practically, Zener introduced the concept of 'frustrating antiferromagnetism' when discussing the *fcc* and *hcp* structures).

In line with the above estimates, see equation (16), Zener's assumption can be discussed on very basic grounds, starting again with equation (1) and supposing that the atoms A and B are well separated, with effective charges $Z_A = Z_B = Z \neq 1$. Then, the absolute values of the coordinate differences $r_{A2} \approx r_{B1} \approx r_{12} \approx r_{AB}$ and the term $(Z - 1)^2 / r_{AB} > 0$ is separated before the integral, which in turn can be further expressed as $|S_{AB}|^2$. Therefore, for large separations, the exchange integral is positive, as for the Bethe-Slater curve and contradicting Zener's hypothesis.

However, by taking the antiferromagnetic coupling between nearest neighbors for granted, Zener turned to the analysis of the coupling of localized d electrons with the delocalized s electron. Spectroscopic data allowed to affirm that always the coupling of an s shell with an incomplete d shell is with parallel spins, even in insulated atoms and ions. Since in the solid state a stronger interaction is expected to occur between these shells, owing to the band overlapping, it is to be expected that the interaction will be fostered in metals with respect to the insulated atoms. Only in the case in which this s-d exchange interaction exceeds the antiferromagnetic direct exchange between neighboring atoms is ferromagnetism expected to occur.

Denoting by S_d the spin of the d shell consisting in localized electrons and by S_c the spin of the s shell ('conduction' electron), Zener proposed a simple formula for the interaction that may lead to ferromagnetism:

$$\Delta E_{ferro.} = \frac{1}{2} \alpha S_d^2 - \beta S_d S_c + \frac{1}{2} \gamma S_c^2 \quad (20)$$

where α characterizes the antiferromagnetic coupling ($\alpha = -4n_d \eta J_{dd}$, where ηJ_{dd} is the Heisenberg interaction with all η neighbors carrying S_d , with $J_{dd} < 0$), β characterizes the ferromagnetic s-d coupling ($\beta S_c = n_d \xi J_{cd} > 0$, where $S_c = \xi/2$), and γ the increase of the kinetic energy induced by the ferromagnetic ordering in the conduction electrons. According to the Stoner ferromagnetism, this term is

$n_c \xi^2 / [4g_c(\epsilon_F)]$, therefore $\gamma = 2n_d/g_c(\epsilon_F)$. For one atom, α is a few eV and should decrease when the overlap between neighboring d shells decrease, e.g. for the transition elements situated at the right-hand side of the periodic table (more electronegative, i.e. when the d shells are more confined towards the nuclei). β is on the order of magnitude of about 1 eV, and may be estimated from spectroscopic data. γ is on the order of magnitude of the Fermi energy divided by the number of conduction electrons per atom, therefore it may also be several eV. By minimizing equation (20) with respect to S_c , one obtains $S_{c, opt.} \approx (\beta/\gamma)S_d$, therefore the average value for the spin projection of the conduction electrons is rather lower than unity. It follows also an expression for the interaction:

$$\Delta E_{ferro.} = \frac{1}{2} \left(\alpha - \frac{\beta^2}{\gamma} \right) S_d^2 \quad (21)$$

A criterion for ferromagnetism, as in the case of the band ferromagnetism, occurs: $\beta^2 > \alpha\gamma$. If ferromagnetism is stable, the parameter $\beta^2/\gamma - \alpha$ may then be interpreted as an ‘exchange integral’ and introduced in the Weiss theory of ferromagnetism. It follows also that this ‘exchange integral’ can take higher values than in the case of direct exchange, a few tenths of eV. Therefore, ferromagnetism in metals might be more robust than in Heisenberg (insulating) systems, and this indeed happens, if one compares the Curie temperature of Fe or Co to that of ferromagnetic oxides.

With his model, Zener introduced the term of ‘indirect exchange’, where the magnetic interaction is transmitted from one spin to another not by direct exchange interaction, but intermediated by a third entity (a conduction electron) able to carry the information about the orientation of one spin to the next one. Variants of the indirect exchange are the ‘superexchange’ where the interaction between two magnetic ions is intermediated by the orbitals of a nonmagnetic ion (typical cases Fe - O - Fe or Mn - O - Mn), leading to ferromagnetic or antiferromagnetic order [18]. Indirect exchange intermediated by the conduction electrons will be treated more extensively in the next Subsection.

By introducing the values for α , β and γ expressed in terms of exchange integrals, density of interacting S_d (i.e. n_d), and density of ‘conduction’ electrons n_c with their asymmetry given by ξ , the optimum asymmetry is obtained as:

$$\xi_{opt.} = 2J_{cd} g_c(\epsilon_F) S_d \left(\frac{n_d}{n_c} \right) \quad (<1) \quad (22)$$

Note that n_d is the density of total atomic spins S_d , coupled according Hund’s rules, and *not* the density of d electrons. For a pure metal, n_d is simply the atomic density, therefore (n_d/n_c) may be regarded as the inverse of the s orbital occupancy $1/\sigma$, where the electronic configuration of the metal with μ outer shell electrons may be written as $4s^\sigma 3d^{\mu-\sigma}$ or $5s^\sigma 4d^{\mu-\sigma}$.

When equation (22) is satisfied, the criterion for Zener ferromagnetism may be written as:

$$J_{cd}^2 g_c(\epsilon_F) > 2\eta |J_{dd}| \left(\frac{n_c}{n_d} \right) \equiv 2\eta |J_{dd}| \sigma \quad (23)$$

Note that the density of states refers to s (or ‘conduction’) electrons only. For ferromagnetism to occur, it is clear that larger ferromagnetic interactions with conduction electrons and larger density of states of these conduction electrons at the Fermi energy are needed; but the surprising result is that the ratio between the density of conduction electrons and that of the localized S_d spins must be low.

By assuming that $\Delta E_{ferro.} = -\lambda \mu_0 \mu_r M^2$, with $M = (n_c \xi_{opt.} + 2 n_d S_d) \mu_B$, the ‘Zener’ molecular field constant can be expressed as:

$$\lambda_Z = \frac{J_{cd}^2 g_c(\varepsilon_F) \left(\frac{n_d}{n_c} \right) - 2\eta |J_{dd}|}{4n_d \mu_0 \mu_r \mu_B^2 (1 + g_c(\varepsilon_F) J_{cd})^2} \approx \frac{1}{4n_d \mu_0 \mu_r \mu_B^2} \left\{ J_{cd}^2 g_c(\varepsilon_F) \left(\frac{n_d}{n_c} \right) - 2\eta |J_{dd}| \right\} \approx \frac{J_{cd}^2 g_c(\varepsilon_F)}{4n_c \mu_0 \mu_r \mu_B^2} \quad (24)$$

where the last approximate relation was written for the case of well separated S_d spins. For practical evaluations, it is always good to know that the density of states for s electrons is a smooth curve, therefore, for nearly half-filled s bands $g_c(\varepsilon_F) \approx 1/W_c$. where W_c is the bandwidth of the conduction electrons (several eV). Numeric estimates give a value of the molecular field constant exceeding one hundred for J_{cd} on the order of 1 eV and the bandwidth on the order of several eV. Note, however, that λ has a quadratic dependence on J_{cd} .

d) A Stoner-Zener model

An immediate development can be made, by integrating the Stoner and the Zener model into a single picture. We consider both the indirect exchange between localized d electrons and conduction s electrons, together with the intrasite repulsion between s electrons. Assuming that the Coulomb repulsion between s and d electrons doesn't have any spin dependence, everything may be written by introducing the Hubbard energy U in the ξ^2 dependent term, by replacing $1/g_c(\varepsilon_F)$ with $1/g_c(\varepsilon_F) - U$. Consequently, the criterion for ferromagnetism (23) is written as:

$$J_{cd}^2 g_c(\varepsilon_F) > 2\eta |J_{dd}| \left(\frac{n_c}{n_d} \right) (1 - U g_c(\varepsilon_F)) \quad (25)$$

and one sees that it is immediately satisfied when only the Stoner criterion is satisfied $U g_c(\varepsilon_F) > 1$. The molecular field constant becomes, in the case where the Stoner criterion is not fulfilled:

$$\lambda_{SZ} = \frac{J_{cd}^2 g_c(\varepsilon_F) \left(\frac{n_d}{n_c} \right) (1 - U g_c(\varepsilon_F)) - 2\eta |J_{dd}| (1 - U g_c(\varepsilon_F))^2}{4n_d \mu_0 \mu_r \mu_B^2 \{1 + (J_{cd} - U) g_c(\varepsilon_F)\}^2} \approx \frac{J_{cd}^2 g_c(\varepsilon_F) (1 - U g_c(\varepsilon_F))}{4n_c \mu_0 \mu_r \mu_B^2 \{1 + (J_{cd} - U) g_c(\varepsilon_F)\}^2} \quad (26)$$

and it has a divergence when $(U - J_{cd})g(\varepsilon_F)$ increases towards unity, which means that the Stoner criterion would be already satisfied. In fact, this divergence does not manifest, since the ‘optimum’ spin asymmetry may be written as:

$$\xi_{opt.} = \frac{2J_{cd} g_c(\varepsilon_F)}{1 - g_c(\varepsilon_F) U} S_d \left(\frac{n_d}{n_c} \right) (< 1) \quad (27)$$

In the following, we consider that the Stoner criterion is not satisfied $g_c(\varepsilon_F) U < 1$. The fact that the optimum spin asymmetry cannot exceed 1 is translated into the following condition:

$$g_c(\varepsilon_F)U < 1 - 2\left(\frac{n_d}{n_c}\right)S_d g_c(\varepsilon_F)J_{cd} \quad (28)$$

If this condition is not fulfilled, then $\xi = 1$ and the maximum asymmetry of conduction electrons is realized. Taking into account both cases from above, one can explicitly write the energy per unit volume as:

$$\Delta E_{ferro} = \begin{cases} n_d \left\{ 2\eta |J_{dd}| - \left(\frac{n_d}{n_c}\right) J_{cd}^2 \frac{g_c(\varepsilon_F)}{1 - U g_c(\varepsilon_F)} \right\} S_d^2, & \text{if equation (28) holds} \\ n_d \left[2\eta |J_{dd}| S_d^2 - J_{cd} |S_d| \right] + \frac{n_c}{4} \left(\frac{1}{g_c(\varepsilon_F)} - U \right), & \text{if equation (28) does not hold} \end{cases} \quad (29)$$

The modulus of S_d in the second equation (29) comes from the symmetry of the problem when the spin is reversed (in that case, ξ_{opt} , according to equation (27), would be lower than -1). It may be seen that, when the Stoner criterion is approached, the energy is minimized when $|S_d|$ shifts from its maximum allowed value from Hund's rules (which would be the case for a simple parabola, when equation (28) holds) to one quarter of the ratio between the indirect exchange interaction and the direct one $S_0 = J_{cd} / (4\eta |J_{dd}|)$, irrespective on the density of spins or of conduction electrons. In general, the second equation (29), when the criterion for ferromagnetism (28) is satisfied, yields a curve with two minima at $\pm S_0$.

Zener and Stoner ferromagnetisms are obtained from the above formula as limiting cases when $U = 0$ or when $J_{cd} = 0$. These derivations are left to the reader as an exercise.

e) Superparamagnetism

For insulated nanoparticles, each one exhibiting ferromagnetic order, individually, a phenomenon called superparamagnetism occurs [19]. This behavior is characterized by an abrupt variation of the $M(H)$ curve, with no hysteresis. It can be well described by a Langevin function: equations (4-5), for large values of the spin S , are written as:

$$M(H) = 2n\mu_B S \times L\left(\frac{2\mu_0\mu_r\mu_B S}{k_B T} H\right) \equiv 2n\mu_B S \coth\left(\frac{2\mu_0\mu_r\mu_B S}{k_B T} H\right) - \frac{nk_B T}{\mu_0\mu_r H} \quad (30)$$

Saturation is reached for low values of the applied field H ($\mu_0 H$ of a few mT), if S exceeds one million. The large value of S is in this case just the total spin of each nanoparticle. In case of distributions of nanoparticles described by known functions, modified formulas may be proposed, see e.g. Ref. [20]. We reconsider the case of the Stoner-Wohlfarth model, for an ensemble of nanoparticles with randomly distributed easy axes, at high temperatures, such that both negative and positive states of magnetization are realized. Averaging equation (12), for the case of no field applied to the system and for $0 \leq \theta \leq 180^\circ$ yields zero permanent magnetization. Cooling down the system 'freezes' this situation with no net magnetization. Then, applying a small magnetic field, such that the Zeeman energy is considerably lower than the anisotropy energy, will not change the situation, at least if the time spent to observe the system is low enough. Despite the fact that in the actual case states with the moments of the nanoparticles oriented more or less along the applied field ($0 < \theta < 90^\circ$) are lower in energy than

the corresponding states with the moments oriented along the angle $180^\circ - \theta$, the thermal fluctuations are not enough to overcome the barrier for the latter cases, and to yield the most favourable energetic state. The time needed to overcome this barrier (the ‘Néel relaxation time’) may be expressed as:

$$\tau_N = \tau_0 \exp\left(\frac{\varepsilon_u N}{k_B T}\right) = \tau_0 \exp\left(\frac{K_u V}{k_B T}\right) \quad (31)$$

where N is the number of spins in the nanoparticle and V its volume. τ_0 is the ‘attempt time’, i.e. the time spent by each nanoparticle between two attempts of switching its orientation in the direction of the most favorable energetic state. Eventually, τ_0 may be connected to the thermal energy $k_B T$ via the uncertainty principle, when speaking about the typical frequency of the driving forces (thermal fluctuations) $\tau_0 \sim h / (k_B T)$, or to the gyromagnetic precession in an applied field B , $\tau_0 \sim h / (\mu_B B)$, when considering the typical response times [21]. Typical orders of magnitude between 10^{-9} to 10^{-13} seconds are obtained for most practical cases.

When the anisotropy energy is large with respect to the thermal energy, the Néel relaxation time may even exceed the estimated age of the Universe. Therefore, once the nanoparticle system is ‘frozen’ e.g. in a state with zero average magnetization, it will remain in this state indefinitely. Applying a small magnetic field and warming up the system implies that, at a given temperature, the system has enough time to ‘relax’ on the measurement time scale and to occupy states energetically more favorable, i.e. with $0 < \theta < 90^\circ$. A non-vanishing magnetization will manifest, therefore in the $M(T)$ curve one observes an increase, $\partial M / \partial T > 0$. For larger temperatures, thermal fluctuations become so important that the average magnetization decreases with temperature, as for a normal paramagnet. Thus, one observes a peak in the ‘zero field cooled’ (ZFC) curve. From the position of this peak, one may estimate the magnetic anisotropy energy, of course, by doing also some suppositions about the ‘attempt time’ and setting the relaxation time to the (presumably known) measurement time. This derivation is, however, hindered also by the fact that in most cases one encounters a distribution of nanoparticles, therefore merely only qualitative derivations are made starting with the peak in the zero field cooled $M(T)$ curves.

When the system of nanoparticles is cooled down in an applied field, above the coercitive field defined e.g. starting with equation (11), the system is ‘frozen’ in a magnetic state and will exhibit a non-vanishing magnetization at low temperature. $M(T)$ increases and stabilizes with decreasing of the temperature, since thermal fluctuations lower in magnitude. No peak should be observed. Anyway, in the following we shall demonstrate that in the case of diluted magnetic semiconductors some non-monotonous behavior of the ‘field cooled’ curve may be observed, and this may be connected to the spin glass or to the indirect exchange character of the magnetic interactions.

f) Spin glasses

Experimentally, the first systems exhibiting ‘spin glass’ behavior were alloys of magnetic elements (Fe, Mn) with noble metals (Cu, Au) [22]. Spin glasses are defined as systems exhibiting a cusp in the magnetic susceptibility, at a ‘glass transition temperature’ T_g . Efforts were undertaken to describe this cusp as a phase transition; however, no other second order derivative of the energy (in particular, the specific heat) was found to present a similar behavior [23]. The Ruderman-Kittel-Kasuya-Yosida (RKKY) theory (sketched in more detail in the next Section) treats the mutual coupling between two insulated spins via the conduction electrons, at a more sophisticated level than the Zener theory. It will be shown that the exchange integrals derived in the RKKY theory oscillate with the separation distance between the two spins, therefore ferromagnetic and antiferromagnetic couplings are equally expected to occur

in such systems. Hence, it is believed that spin glasses may be modeled as ensembles of spins with either ferromagnetic or antiferromagnetic couplings between them; it is easy to see that most of these systems will be ‘frustrated’, i.e. one may find a closed path starting with one spin, going from one spin to another and ordering all time the current spin according to the coupling with the previous one, ending with the necessity of reversing the spin of the initial spin (the reader can just investigate mentally the possibility of antiferromagnetic coupling in a *fcc* or *hcp* lattice). Thus, in contrast with the ferromagnetic case, these systems will possess intrinsic disorder, manifested in random signs of the exchange integrals J_{ij} . The Edwards-Anderson theory [23] treats oscillating interactions between spins dissolved in the matrix, with the result of no mean ferro- or antiferromagnetism, but with identification of a ground state with the spins aligned in definite directions, even if these directions appear to be at random. “At the critical temperature the existence of these preferred directions affects the orientation of the spins, leading to a cusp in the susceptibility.” [23]. The Sherrington-Kirkpatrick (SK) theory [24] starts with a gaussian distribution of exchange integrals between spins, uses the ‘replica trick’ and ends up with the derivation of a phase diagram of the three possible states: paramagnetism, spin glass, and ferromagnetism, as function on the mean exchange integral, width of the distribution of the exchange integral, and thermal energy. The spin glass state is characterized by no net magnetization $m = \langle S \rangle = 0$, but nonvanishing average value of the correlation functions $\langle S_i(t_1)S_j(t_2) \rangle$. The magnetic susceptibility and the specific heat present cusps at T_g , while the zero temperature entropy becomes negative in SK theory. In Ref. [24], it is commented that these unphysical results may occur from some problems when the thermodynamical limit $N \rightarrow \infty$ is interverted with the ‘replica limit’, that is, the number of replicas should vanish.

A more terrestrial point of view was presented by Trachenko in Ref. [25], where the possibility of a phase transition is simply discarded and the considerations we employed at the description of relaxation effects in zero field cooled superparamagnetic nanoparticles are considered also in this case. At high temperature, the system is paramagnetic and the susceptibility obeys the Curie law $\chi = C/T$. At low temperature, spins are frozen and subject to periodic attempts to be re-arranged in the direction of the applied field. The microscopic mechanism coupling thermal agitation with spins are the spin waves, which can be shown to yield a parabolic dependence of the susceptibility on the temperature $\chi = \chi_0 + AT^2$. This qualitatively describes the cusp in the susceptibility curve, with T_g defined as the temperature from which spins are able to rotate and to fully relax in the direction of the applied field. At low temperatures, spins just oscillate, attempting to align in the direction of the applied field, and only a minor part of them succeed. This is the origin of the lower susceptibility in the ‘frozen’ state.

RKKY interaction

The semiconductors are special cases, situated from their conduction properties between the metals and the insulators. If we take for granted that in magnetic insulators the magnetism occurs by direct (Heisenberg) exchange, eventually by superexchange, whereas in metals delocalized electrons are involved, with ferromagnetism occurring either owing to the Coulomb intrasite repulsion, or to the coupling of localized spins with delocalized electrons, it is difficult to anticipate which mechanism will prevail in the case of semiconductors. The Zener model seems a promising candidate, but it is easy to see from the above formulas (20-27) that both the molecular field constant and the deepness of the potential well $\Delta E_{ferro}(S_d)$, which is suspected to characterize the stability of the ferromagnetic phase, decrease by increasing the density of delocalized charge carriers n_c . Typically, in semiconductors $n_c \sim 10^{18} - 10^{25} \text{ m}^{-3}$, whereas for achieving a diluted magnetic semiconductor with observable and usable magnetic properties, a minimum doping with magnetic ions of a few atomic percents is needed. Consequently, $n_d \sim 10^{27} - 10^{28} \text{ m}^{-3}$, therefore the ratio (n_c/n_d) will be low. Also, one generally uses

doping atoms with as large as possible individual moments (from Cr with $S_d^{(\max)} = 5/2$ to Co with $S_d^{(\max)} = 1$). In these conditions, equations (20) or (25) yield large values for ξ_{opt} , thus one has to infer that the conduction electrons are fully spin polarized $\xi = 1$. In the case of presence or absence of the antiferromagnetic coupling $J_{dd} < 0$, the atomic energy barrier will be given by:

$$\frac{\Delta E_b}{n_d} = \begin{cases} \frac{J_{cd}^2}{2\eta|J_{dd}|} - \left(\frac{n_c}{n_d}\right) \frac{1 - Ug_c(\epsilon_F)}{g_c(\epsilon_F)} \approx \frac{J_{cd}^2}{2\eta|J_{dd}|}, & \text{if } J_{dd} \neq 0 \\ J_{cd}S_d^{(\max)} - \left(\frac{n_c}{4n_d}\right) \frac{1 - Ug_c(\epsilon_F)}{g_c(\epsilon_F)} \approx J_{cd}S_d^{(\max)}, & \text{if } J_{dd} = 0 \end{cases} \quad (32)$$

If $J_{dd} \neq 0$, the local minima are realized at $\pm J_{cd} / (4\eta|J_{dd}|)$, whereas if $J_{dd} = 0$ the minimum energy is realized for maximum absolute value $S_d^{(\max)}$.

The consequence of the above formula is that, in the framework of the Zener model, there is little hope to control the stability of the ferromagnetism by varying the density of charge carriers. If, additionally, the magnetic impurities are donors or acceptors, $n_c = n_c^{(0)} + \delta n$, with $n_c^{(0)}$ the electron or hole concentration induced by the magnetic ions, and δn the electron or hole concentration which can be modulated by external parameters. Now, $n_c^{(0)}$ will be on the order of n_d , and $\delta n \ll n_d$. Finally, a similar effect will be obtained, in the low possibility of ferromagnetism control via the modulable density of carriers in the semiconductor. This is the reason for which we tackle in this paragraph a more sophisticated, widely accepted model in the physics of diluted magnetic semiconductors.

The RKKY model was proposed in the 1950's by Ruderman, Kittel, Kasuya and Yosida [26-28] and analyzes again the coupling between the individual spin moments by conduction electrons. In the following, we shall sketch a brief derivation of the RKKY formula, starting with perturbation theory.

a) The s-d exchange integral

Let us set atom A in the origin, and consider a localized electron described by the Wannier (atomiclike) function $\Psi_A(\mathbf{r}) \equiv \phi_0(\mathbf{r})$. Consider a second electron described by a Bloch function $\phi_b(\mathbf{r})$ [29]:

$$\phi_b(\mathbf{r}) \equiv \psi_k(\mathbf{r}) = \frac{1}{\sqrt{\Omega}} \phi_k(\mathbf{r}) = \frac{1}{\sqrt{\Omega}} \exp(i\mathbf{k} \cdot \mathbf{r}) u_k(\mathbf{r}) \quad (33)$$

normalized such as $\int d^3r |\phi_k(\mathbf{r})|^2 = \Omega = \int d^3r |u_k(\mathbf{r})|^2$, where Ω is the volume of the crystal. We neglect the first three terms from (1), by considering atom B far apart from atom A. Thus, $R_B \rightarrow \infty$ and the terms with R_{AB}^{-1} and r_{B1}^{-1} vanish in (1). The term containing r_{A2}^{-1} may be shown to vanish owing to the d character of $\phi_0(\mathbf{r})$ combined with its localized character. Indeed, an integral such that $\int d^3r u_k^*(\mathbf{r}) \exp(-i\mathbf{k} \cdot \mathbf{r}) (-Z/r) \phi_0(\mathbf{r})$ must be computed: the exponential may be developed in series, the z axis is chosen along the direction of \mathbf{k} , and the first two terms of the development of the exponential are orthogonal to $\phi_0(\mathbf{r})$. This approximation is valid for $kR_0 \ll 1$, where R_0 is the dimension of the state ϕ_0 (see below). At the end of the actual derivation, we will prove the fact that the interesting values of the wavevector k are related to the inverse of the separation between two insulated magnetic ions, i.e. k is much lower than the inverse of the estimate 'dimension of ϕ_0 '.

The last term of the exchange integral (1) is written as:

$$J_{kk} = \frac{1}{\Omega} \int d^3r_1 d^3r_2 \frac{e_0^2 \phi_0^*(r_1) \phi_k^*(r_2) \phi_0(r_2) \phi_k(r_1)}{r_{12}} \quad (34)$$

Let \mathbf{S} be the spin of the Bloch electron, and \mathbf{S}_0 the localized spin. The Heisenberg exchange energy may be written as the mean value of the 'exchange operator' $\hat{\Delta}$:

$$-2J_{kk} \mathbf{S} \cdot \mathbf{S}_0 = -\frac{2\mathbf{S} \cdot \mathbf{S}_0}{\Omega} \langle \phi_k(\mathbf{r}) | \hat{\Delta} | \phi_k(\mathbf{r}) \rangle \quad (35)$$

while this operator acts following the rule:

$$\hat{\Delta} \phi_k(\mathbf{r}) = \int d^3r' \frac{e_0^2 \phi_0^*(\mathbf{r}') \phi_k(\mathbf{r}') \phi_0(\mathbf{r})}{|\mathbf{r} - \mathbf{r}'|} \quad (36)$$

In the following, we evaluate the intensity of the double exchange interaction. Let us set $u_k = \text{const.}$ in the Bloch function (29) and consider $\phi_0(\mathbf{r})$ confined inside a sphere of radius R_0 , and volume w_0 . It follows $\langle \hat{\Delta} \rangle \approx 3e_0^2 w_0 / (2R_0)$. The order of magnitude of the double exchange interaction is the volume of the localized state times the Coulomb energy corresponding to that state. If $R_0 \approx 1$ Bohr radius (a_B), one obtains about $3 \text{ Ry} \times w_0$, where $e_0^2 / a_B = 2 \text{ Ry} \approx 27.2 \text{ eV}$. For a comparison with the orders of magnitude encountered previously for direct exchange interactions, one has to sum this energy over all electrons from the crystal (N) and divide by the total volume of the crystal. A factor Nw_0/Ω occurs, which may be regarded as the 'filling' of the crystal with localized electrons. For $R_0 \approx 2 a_B$ and the volume of a Wigner-Seitz cell of about $125 a_B^3$, one obtains an estimate for the indirect exchange energy of 1.4 eV , which is a robust value.

b) Perturbation theory

A further approximation made in the derivation of the RKKY interaction is the use of non-degenerate perturbation theory for the Bloch functions, although it is clear that the energy spectrum of electrons in a crystal is rather degenerated (e.g. for free electrons there is a complete angle degeneracy, for tight binding theory there is also degeneracy, etc.)

In the following, we recall briefly the results of the non-degenerate perturbation theory. When the Hamiltonian of a system may be expressed as $\hat{H} = \hat{H}_0 + \hat{H}_1$, where for the first term one knows the eigenfunctions and eigenvalues $\hat{H}_0 \psi_i^{(0)} = E_{0i} \psi_i^{(0)}$, with normalization $\langle \psi_i^{(0)} | \psi_j^{(0)} \rangle = \delta_{ij}$, and the second term \hat{H}_1 can be treated as a perturbation, the energy and the wavefunction of the system may be developed in series on the 'order of perturbation':

$$E_n = \sum_{j=0}^{\infty} E_n^{(j)} ; \quad \psi_n = \sum_{j=0}^{\infty} \psi_n^{(j)} \quad (37)$$

The first orders of perturbation theory give the following results:

i) 0th order: the energy is that of an eigenstate n $E_n^{(0)} = E_{0n}$, the wavefunction is one of the eigenfunctions of \hat{H}_0 : $\psi_n^{(0)}$.

ii) 1st order: the energy correction is the average of the perturbation computed on the unperturbed state:

$$E_n^{(1)} = \langle \psi_n^{(0)} | \hat{H}_1 | \psi_n^{(0)} \rangle; \text{ the wavefunction is: } \psi_n^{(1)} = \sum_{k \neq n} \frac{\langle \psi_k^{(0)} | \hat{H}_1 | \psi_n^{(0)} \rangle}{E_n^{(0)} - E_k^{(0)}} \psi_k^{(0)} \quad (38.1)$$

iii) 2nd order [30]:

$$E_n^{(2)} = \sum_{k \neq n} \frac{|\langle \psi_k^{(0)} | \hat{H}_1 | \psi_n^{(0)} \rangle|^2}{E_n^{(0)} - E_k^{(0)}} \quad (38.2)$$

$$\psi_n^{(2)} = \sum_{l \neq n} \left[\sum_{k \neq n} \frac{\langle \psi_l^{(0)} | \hat{H}_1 | \psi_k^{(0)} \rangle \langle \psi_k^{(0)} | \hat{H}_1 | \psi_n^{(0)} \rangle}{(E_n^{(0)} - E_l^{(0)})(E_n^{(0)} - E_k^{(0)})} - \frac{\langle \psi_n^{(0)} | \hat{H}_1 | \psi_n^{(0)} \rangle \langle \psi_l^{(0)} | \hat{H}_1 | \psi_n^{(0)} \rangle}{(E_n^{(0)} - E_l^{(0)})^2} \right] \psi_k^{(0)} - \frac{1}{2} \sum_{k \neq n} \frac{|\langle \psi_k^{(0)} | \hat{H}_1 | \psi_n^{(0)} \rangle|^2}{E_n^{(0)} - E_k^{(0)}} \psi_k^{(0)} \quad (38.3)$$

We apply now this theory for computing the influence of the exchange operator $\hat{\Delta}$ on the system described by Bloch electrons interacting with localized electrons.

Let us first remark that in the 1st order one obtains a contribution to the energy resembling equation (35), containing the scalar product between the localized spin \mathbf{S}_0 and the spin of the itinerant electron \mathbf{S} . This contribution vanishes when one sums over the orientations of \mathbf{S} , in other words one considers that the itinerant electrons are not spin polarized ($n_\uparrow = n_\downarrow$) which, of course, consists an approximation even with respect to the Zener model. In the case $n_\uparrow \neq n_\downarrow$, when Stoner ferromagnetism manifests [15], the first order correction in perturbation theory might not be neglectible.

Back to the RKKY model, one considers the interaction Hamiltonian as being the sum of two contributions, corresponding to localized electrons situated at two different sites, 1 and 2: $-2\mathbf{S}_1 \cdot \mathbf{S}_0 \hat{\Delta}_1 - 2\mathbf{S}_2 \cdot \mathbf{S}_0 \hat{\Delta}_2$. The indices 1 and 2 refer to the origin of the Wannier function in the equilibrium position of the two atoms $\phi_0(\mathbf{r} - \mathbf{R}_1)$ and $\phi_0(\mathbf{r} - \mathbf{R}_2)$. We write down now the 2nd order correction to the energy. It is straightforward that in the sum (38.2) components such as $(\mathbf{S}_1 \cdot \mathbf{S})^2$, $(\mathbf{S}_2 \cdot \mathbf{S})^2$ or $(\mathbf{S}_1 \cdot \mathbf{S})(\mathbf{S}_1 \cdot \mathbf{S})$ appear. Terms containing the first two factors are not interesting for the problem of coupling between \mathbf{S}_1 and \mathbf{S}_2 , therefore only crossed terms will be retained from the sum. The energy correction may be written as:

$$\delta E_n^{(2)} = \sum_{k \neq k'} \frac{\langle \psi_{k'}^{(0)} | \mathbf{S} \cdot \mathbf{S}_1 \hat{\Delta}_1 | \psi_k^{(0)} \rangle \langle \psi_k^{(0)} | \mathbf{S} \cdot \mathbf{S}_2 \hat{\Delta}_2 | \psi_{k'}^{(0)} \rangle}{\varepsilon(\mathbf{k}) - \varepsilon(\mathbf{k}')} + \text{c.c} \quad (39)$$

This is valid for the interaction between \mathbf{S}_1 and \mathbf{S}_2 , intermediated by one Bloch electron. The total interaction is computed by summing over all Bloch electrons:

$$E(\mathbf{S}_1, \mathbf{S}_2) = - \sum_{\mathbf{k}, \mathbf{S}} (\mathbf{S} \cdot \mathbf{S}_1)(\mathbf{S} \cdot \mathbf{S}_2) \sum_{\mathbf{k}' \neq \mathbf{k}} \frac{\langle \psi_{\mathbf{k}'}^{(0)} | \hat{\Delta}_1 | \psi_{\mathbf{k}}^{(0)} \rangle \langle \psi_{\mathbf{k}}^{(0)} | \hat{\Delta}_2 | \psi_{\mathbf{k}'}^{(0)} \rangle}{\varepsilon(\mathbf{k}') - \varepsilon(\mathbf{k})} + \text{c.c.} \quad (40)$$

In Ref. [26], a similar expression is obtained starting with collision theory, but we considered that the actual treatment is more rigorous and also allows the explicitation of the exchange operator, together with the evaluation of its matrix elements.

Summing over \mathbf{S} transforms the front factor in $(\mathbf{S}_1 \cdot \mathbf{S}_2)/2$. The sum over the wavevectors \mathbf{k} becomes an integral following the well-defined rules from solid state theory. In order to compute the matrix elements, one uses again the localization property of the Wannier functions, which allows the factorization and removal from the integral of the plane wave component of the Bloch functions, according to the rule:

$$\langle \psi_{\mathbf{k}'}^{(0)} | \hat{\Delta}_j | \psi_{\mathbf{k}}^{(0)} \rangle \approx \frac{1}{\Omega} \exp[i(\mathbf{k}' - \mathbf{k}) \cdot \mathbf{R}_j] \langle u_{\mathbf{k}'} | \hat{\Delta} | u_{\mathbf{k}} \rangle \equiv \frac{1}{\Omega} \exp[i(\mathbf{k}' - \mathbf{k}) \cdot \mathbf{R}_j] \Delta_{\mathbf{k}\mathbf{k}'} \quad (41)$$

with $j=1,2$ and $\mathbf{R}_{12} = \mathbf{R}_2 - \mathbf{R}_1$. A formula is obtained, which in fact is the starting formula from Ref. [26]:

$$E(\mathbf{S}_1, \mathbf{S}_2, \mathbf{R}_{12}) = - \frac{\mathbf{S}_1 \cdot \mathbf{S}_2}{2} \int \frac{d^3 k}{(2\pi)^3} \int \frac{d^3 k'}{(2\pi)^3} \cdot \frac{\Delta_{\mathbf{k}\mathbf{k}'} \Delta_{\mathbf{k}'\mathbf{k}} \exp[i(\mathbf{k} - \mathbf{k}') \cdot \mathbf{R}_{12}]}{\varepsilon(\mathbf{k}') - \varepsilon(\mathbf{k})} + \text{c.c.} \quad (42)$$

c) Computing the RKKY interaction. Orders of magnitude

In the following, two more approximations are made: (i) One considers the matrix elements of the exchange operator as a weakly varying function on \mathbf{k} and, since the most important contribution to the integral (42) comes from the region near the Fermi energy $\mathbf{k} \sim \mathbf{k}' \sim \mathbf{k}_F$, one approximates $\Delta_{\mathbf{k}\mathbf{k}'} \Delta_{\mathbf{k}'\mathbf{k}} \approx |\Delta_{\mathbf{k}\mathbf{k}_F}|^2 \equiv |\Delta|^2$. (ii) One considers that the conduction electrons are behaving like free particles in the crystal, with a dispersion law such as $\varepsilon(\mathbf{k}) = \varepsilon(k) = \hbar^2 k^2 / (2m^*)$, with constant effective mass m^* .

The final result, as derived in Ref. [26], is:

$$E(\mathbf{S}_1 \cdot \mathbf{S}_2, k_F, R_{12}) = - \frac{\mathbf{S}_1 \cdot \mathbf{S}_2}{4} \frac{|\Delta|^2 m^*}{(2\pi)^3 R_{12}^4 \hbar^2} [2k_F R_{12} \cos(2k_F R_{12}) - \sin(2k_F R_{12})] \quad (43)$$

For estimating orders of magnitude, we recall from above that $|\Delta|$ is about 3 Ryd $\times w_0$. One uses 1 Ryd. = $\hbar^2 / (2ma_0^2)$, and for $R_0 = a_B$, the constant before the oscillating function $x \cos(x) - \sin(x)$, where $x = 2k_F R_{12}$, without the spin factor $(\mathbf{S}_1 \cdot \mathbf{S}_2)$, is found as being about 86 meV $\times (a_B / R_{12})^4$.

The next step is to compute the equivalent of the molecular field constant. In this case, one has to average over all spins \mathbf{S}_2 from the solid around \mathbf{S}_1 . Assuming that these spins are uniformly distributed in the solid, with the density n_s and by using a continuous limit, the integral of (43) in spherical coordinates can be solved exactly, by noticing that $(\sin x/x)' = (x \cos x - \sin x)/x^2$. It follows that, if one supposes that all spins \mathbf{S}_2 are aligned, the most favorable state implies an antiferromagnetic ordering of \mathbf{S}_1 with all \mathbf{S}_2 's. If in the integral one introduces a lower cutoff distance R_0 , assuming that

spins cannot be separated by a lower distance than R_0 , the total interaction is described as:

$$E(\mathbf{S}_1 \cdot \mathbf{S}_2, k_F, R_0) = \frac{\mathbf{S}_1 \cdot \mathbf{S}_2}{2} \frac{|\Delta|^2 m^*}{h^2 R_0} n_S \sin(2k_F R_0) \quad (44)$$

and this makes sense only when $\sin(2k_F R_0) < 0$, since we supposed that the system is ferromagnetic, by considering all spins \mathbf{S}_2 aligned. The first region where this happens is $\pi < 2k_F R_0 < 2\pi$.

Another development can be made, by assuming that \mathbf{S}_2 spins are oriented ferromagnetic or antiferromagnetic with respect to \mathbf{S}_1 , according to the sign of the exchange integral. This implies the evaluation of:

$$E(k_F, R_{12}) = -S_1 S_2 \frac{|\Delta|^2 m^*}{h^2} k_F n_S \int_{(R_0 \text{ or } 0)}^{\infty} \frac{|x \cos x - \sin x|}{x^2} dx \quad (45)$$

This energy is always negative, i.e. the apparition of the RKKY interaction implies a state more stable energetically. But here anything can no longer be said on the occurrence of ferromagnetism or antiferromagnetism in the system (both kind of couplings occur), not to speak that frustration was not taken into account.

Finally, a last approximation which may be discussed is to suppose that each spin \mathbf{S}_1 interacts with the η nearest neighbouring spins \mathbf{S}_2 , placed at an average distance R_0 . Assume that $\mathbf{S}_2 = \langle \mathbf{S} \rangle$, then a Weiss-like interaction (per unit volume) is derived:

$$\Delta E_{ferro}(k_F, R_{12}) = -\frac{\mathbf{S} \cdot \langle \mathbf{S} \rangle}{4} \frac{\eta |\Delta|^2 m^*}{(2\pi)^3 R_0^4 \hbar^2} n_S [2k_F R_0 \cos(2k_F R_0) - \sin(2k_F R_0)] \quad (46)$$

which, of course, makes sense only when the oscillating function inside the square brackets is positive, i.e., for instance, the first region where this happens is $4.493 < 2k_F R_0 < 7.725$ (solutions of $\tan x = x$). The molecular field constant, starting with equation (44), may be written as:

$$\lambda_{\text{RKKY}} = -\frac{1}{8\mu_0 \mu_r \mu_B^2} \frac{|\Delta|^2 m^*}{h^2 R_0} \sin(2k_F R_0) = -\frac{1}{8\mu_0 \mu_r \mu_B^2} \frac{|\Delta|^2 m^*}{h^2} n_S^{1/3} \sin \left\{ 2 \left[3\pi^2 \left(\frac{n_c}{n_S} \right) \right]^{1/3} \right\} \quad (47)$$

where the formula connecting the Fermi wavevector and the density of free carriers in a solid, in the free electron approximation $k_F = (3\pi^2 n_c)^{1/3}$ was used, together with the assertion that $n_S \approx R_0^{-3}$.

Starting with equation (45), the molecular field constant yields:

$$\begin{aligned} \lambda_{\text{RKKY}} &= \frac{1}{16n_S \mu_0 \mu_r \mu_B^2} \frac{\eta |\Delta|^2 m^*}{2\pi R_0^4 \hbar^2} [2k_F R_0 \cos(2k_F R_0) - \sin(2k_F R_0)] \\ &= \frac{1}{16\mu_0 \mu_r \mu_B^2} \frac{\eta |\Delta|^2 m^*}{2\pi \hbar^2} n_S^{1/3} \left\{ 2 \left[3\pi^2 \left(\frac{n_c}{n_S} \right) \right]^{1/3} \cos \left\{ 2 \left[3\pi^2 \left(\frac{n_c}{n_S} \right) \right]^{1/3} \right\} - \sin \left\{ 2 \left[3\pi^2 \left(\frac{n_c}{n_S} \right) \right]^{1/3} \right\} \right\} \quad (48) \end{aligned}$$

Of course, in both cases, one needs to consider only situations with $\lambda > 0$. It is interesting to note that, in the case of equation (47), which is obtained by integration over the whole system of spins \mathbf{S}_2 , with

the introduction of a minimum cutoff R_0 , the molecular field constant does not depend on the density of spins and has a weak dependence on the density of conduction electrons. The case when the closest neighbors are considered only, equation (48), has a more complicated dependence.

For $m^* = m_e$ (electron's rest mass) and for the above evaluation for Δ ($3 \text{ Ry} \times w_0$, with w_0 the volume of a sphere of radius a_B), it follows that the molecular field constant may be important in the case of RKKY interaction, yielding e.g. $350 \times \sin(2k_F R_0) / R_0(\text{\AA})$ from equation (46). A mutual average separation between spins of 1 nm leads to quite rectangular hysteresis loops. From equation (47), similar values are obtained, just a factor $\eta/(2\pi)$ appears additionally, before the oscillating function.

Equations (47-48) are exactly what we desired at the beginning of this study, expressions for the 'molecular field constant' connected to the density of charge carriers in the semiconductor. These dependencies are represented in Figure 4.4.

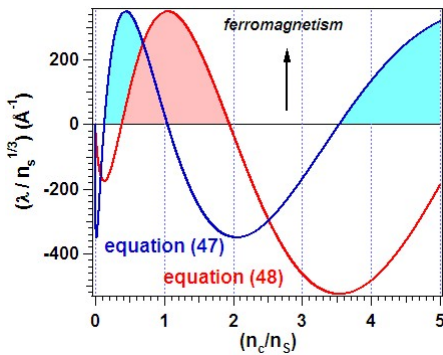


FIGURE 4.4

Molecular field constants obtained from the RKKY theory, according to two ways to estimate the total interaction of a spin with the others: (a) evaluation of the total interaction, with a cutoff at a minimum distance R_0 , connected to the density of spins such as $n_s \approx R_0^{-3}$, yielding equation (47); (b) keeping just the interaction with nearest-neighbors, situated at the distance R_0 , yielding equation (48). η was set to 1 and the multiplicative factor results from the evaluations described in the text

According to equation (47), ferromagnetism occurs if $0.13 < (n_c/n_s) < 1.05$. According to equation (48), one needs $0.38 < (n_c/n_s) < 1.95$. The criterion for Zener ferromagnetism, equation (23), yields $(n_c/n_d) < J_{cd}^2 / (2\eta J_{dd} W) \approx 0.01-0.1$, where $W = 1/g_c(\epsilon_F)$ is the bandwidth of the s electrons. The ranges of the ratio between the density of conduction electrons and that of spins is different from the Zener model to the RKKY. On the other hand, most metals, when introduced into semiconductors, are strong dopants (most often acceptors, but also sometimes donors), therefore n_c/n_s is closer to 1 than to 0.01-0.1. Therefore, the RKKY model seems more appropriate to describe ferromagnetism in diluted magnetic semiconductors than the more empirical Zener model.

The big success during the last decade in synthesizing II-VI or, more specifically, oxide diluted magnetic semiconductors suggests that even when n_c/n_s exceeds 1, ferromagnetism occurs. Therefore, it seems that the model described by equation (48), which is, finally, just the RKKY interaction without any averaging, by considering only closest magnetic impurities, is more appropriate. In the following, we shall investigate in the framework of the present theory the case of Mn diluted in germanium. It will be seen that all concepts developed so far: Zener and RKKY indirect exchange, together with superparamagnetism and spin glasses, will be employed in order to explain the experimental data.

Summary of exchange mechanisms and their fingerprints in $M(H, T)$ behaviors

The magnetization dependence on temperature may be extracted from equation (9), while the remanent magnetization and the coercive field are expressed by equations (8). In these equations, two parameters are important, denoted by a and b . We recall that $b = \mu_0 \mu_r n \mu_{\max}^2 / k_B T$, therefore b may be expressed as T_0/T , with a straightforward significance of T_0 . The parameter a is b times the molecular field constant $a = b\lambda$, and λ , in some models (Zener and RKKY), is also dependent on temperature via the density of charge carriers in the semiconductor n_c . For n or p doped semiconductors, the concentration of charge carriers may be extracted from the neutrality condition in the semiconductor [31]:

$$n = \frac{2N_D}{1 + \sqrt{1 + \frac{8N_D}{N_c} \exp\left(\frac{E_c - E_D}{k_B T}\right)}} \quad p = \frac{2N_A}{1 + \sqrt{1 + \frac{8N_A}{N_v} \exp\left(\frac{E_A - E_v}{k_B T}\right)}} \quad (49)$$

where E_D (E_A) represent donor (acceptor) levels, E_c is the conduction band minimum, E_v the valence band maximum, N_D (N_A) the concentration of donors or acceptors, and N_c (N_v) the conduction (valence) density of states (per unit volume, not per unit energy). Integrating formulas from (49), no matter which is the conduction type, into the Zener or Stoner-Zener molecular field constant (24) or (26) yields the following dependence of a :

$$a_z = \frac{K_0}{T} \left(1 + \sqrt{1 + K_1 \exp\left(\frac{K_2}{T}\right)} \right) - \frac{K_3}{T} \quad (50)$$

An eventual existence of a constant density of charge carriers superposed to the density whose characteristic is semiconductor-like is absorbed into the term K_3/T , which contains also an eventual direct exchange interaction between the spins.

For the RKKY model, the dependence is slightly more complicated:

$$a_{\text{RKKY}}^{(1,2)} = \frac{K_0}{T} F^{(1,2)} \left\{ 2 \left[\left[\frac{K_1}{1 + \sqrt{1 + K_2 \exp\left(\frac{K_3}{T}\right)}} + K_4 \right] \right]^{1/3} \right\} + \frac{K_5}{T} \quad (51)$$

where the eventual existence of a constant density of charge carriers is expressed by the constant K_4 , and an eventual direct exchange interaction is expressed into the constant K_5 . The function $F^{(1,2)}(x)$ is either $(-\sin x)$, or $(x \cos x - \sin x)$, if formulas (47) or (48) are used, respectively.

The above formulas admit simplifications for high temperature, low temperature cases or for high doping levels (degenerate semiconductors). However, in the following we shall use these general formulas, by taking advantage of the actual state of computing machines in performing simulations of the experimental curves.

The case of manganese diluted into Ge(001)

Overview

As mentioned in the Introduction, amongst diluted magnetic semiconductors, Mn_xGe_{1-x} is a promising candidate owing to its high Curie temperature [32,33]. Surface science techniques often succeeded in the past in stabilizing metastable phases of manganese with ferromagnetic or ferrimagnetic properties [34-36]. In germanium, solid state compounds such as $Mn_{13}Ge_4$, $Mn_{11}Ge_8$, Mn_5Ge_2 , Mn_5Ge_3 , Mn_3Ge_2 are known to date [37], of which only Mn_5Ge_3 is reported to be ferromagnetic. This compound seems to be the origin of the detected ferromagnetism in Mn-Ge 'diluted magnetic semiconductors' [38-40]. Hence, despite the relative success in stabilizing ferromagnetic Mn-based phases on Ge(111) [35,36,38,39,41], it is highly desirable to find a simpler route to synthesize Ge-Mn-based compounds, possibly richer in germanium, in order to provide less metallic character, to offer the possibility of triggering ferromagnetism by varying the charge carriers, and to be appropriate for integration with Si-based electronics.

Some recent reports demonstrated enhanced magnetic properties just by annealing to promote Mn interdiffusion with Ge [42]. Superparamagnetic Mn-Ge compounds are reported [43] and might be appropriate for applications in magnetic sensors directly integrated on semiconductors [32]. Note also that the interesting surface for applications in microelectronics is Ge(001), whereas the majority of studies that succeeded to stabilize Mn-based ferromagnetic compounds processed the Ge(111) surface up to now.

Recently, room temperature ferromagnetism in Mn:Ge(001) systems via a 'subsurfactant epitaxy' method subsequent to the deposition half a monolayer of Mn on Ge(001) was achieved [36]; however, in this case, the relatively low Mn content obtained (about 0.25 %) precludes further applications in magnetic devices. The synthesis of a Ge-rich phase ($\sim MnGe_2$) was also achieved, organized in nanocolumns, providing a Curie temperature over 400 K [44]. However, a previous work from the same team on such columnar structures did not succeed to synthesize room temperature ferromagnetic material [36,45]. This points out the quite delicate conditions required by using co-evaporation of manganese and germanium on Ge(001) in order to achieve robust magnetism. Also, connected to Section 2, it might be inferred that the oscillatory character of the RKKY interaction makes the occurrence of ferromagnetism quite delicate.

A simpler route for synthesizing such magnetic systems is the 'solid phase epitaxy' [40,46], where Mn is simply deposited on Ge single crystals either at room temperature, with subsequent annealing, either directly at a more elevated temperature. So far, results were reported on Ge(111) surfaces [35,46-49]. A Mn_5Ge_3 -induced superstructure of $(\sqrt{3} \times \sqrt{3})R 30^\circ$ was observed by reflection high energy electron diffraction (RHEED) in [35,46], and by low energy electron diffraction (LEED) in [47], whereas all reports point on a strong decrease of the saturation magnetization near room temperature. Nevertheless, room temperature ferromagnetism was reported in Refs. [40,47,49] and a weak magnetic moment at room temperature seems also to be provided by the studies reported Ref. [46]. Comparatively, there are no reports on surface structure or eventual reconstructions, nor on magnetic properties for Ge(001) subject to a solid phase epitaxy, despite the fact that this surface may be connected to the technologically important Si(001) surface.

In the following, we will report on LEED and high resolution transmission electron microscopy (HRTEM) observations, together with superconducting quantum interference device (SQUID) measurements on Ge(001) subject to Mn deposition at relatively high temperatures (250-350 °C). Below 250 °C substrate temperatures, no room temperature ferromagnetism is detected. The preservation of the Ge(001)

surface upon deposition of a considerable amount of Mn (the equivalent of 100 nm of bulk manganese) is observed, together with a ferromagnetic hysteresis loop at room temperature.

Structure and morphology (LEED, HRTEM)

In Ref. [47], Fe layers of up to 12 ML ($\approx 17 \text{ \AA}$) were deposited on Ge(001) at 500 °C and the LEED images still exhibited a clear (1 x 1) pattern, which is a sign of Fe diffusion inside the Ge single crystal. This result is at variance with similar experiments on Si(001), where Fe deposited at room temperature did not show any LEED pattern, and at high temperature exhibited some spots only for very few layers deposited [48,49]. The case of Sm deposited on Si(001) was more promising, in the fact that broad LEED spots were visible for high temperature depositions (300 °C) up to $\sim 3 \text{ nm}$ effective Sm thickness [50,51]. Therefore, as a general rule, deposition of highly reactive metals (which is the case of magnetic metals, owing to their incomplete valence shells) on semiconductors strongly affects the semiconductor surface and promotes the formation of various interface compounds.

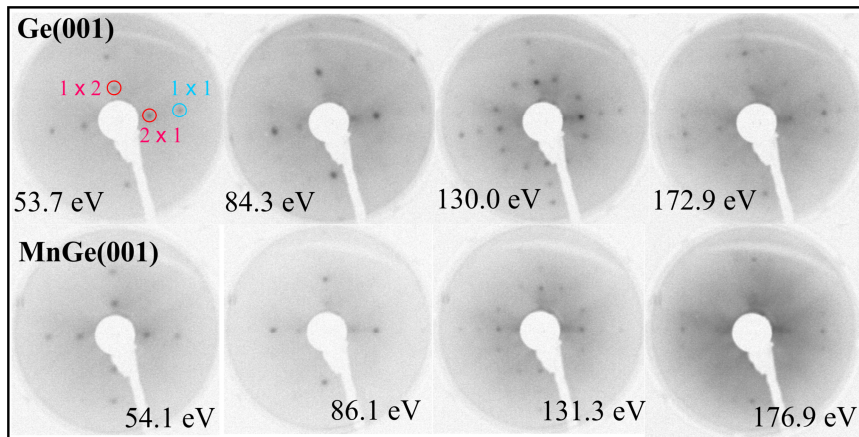


FIGURE 4.5

Low energy electron diffraction (LEED) patterns for Ge(001) on the panels above, and for Mn deposited on Ge(001) at 350 °C (panels below). Each image is indexed with the energy of incoming electrons. For better clarity, negative images of the true LEED photographs are displayed. The (1 x 1), (2 x 1) and (1 x 2) spots are highlighted on one LEED image for clean Ge(001). Reproduced from Ref. [52]

The case of manganese deposition on Ge(001) (2 x 1) was surprising, as compared to the above situations. Figure 4.5 presents LEED patterns obtained on clean Ge(001) wafers and after the deposition of a huge amount (the equivalent of 100 nm) of Mn at 350 °C substrate temperature [52]. One can see that not only the surface is ordered, but even the (2 x 1) reconstruction is preserved. Ref. [52] presents also scanning tunneling microscopy (STM) images, where the Ge dimers were visible also on the surface after Mn deposition, only the Ge-Ge distance of these dimers increased slightly over Mn deposition. This is an immediate evidence that manganese diffuses deep inside the Ge(001) wafer, preserving its surface. Therefore, the Mn-Ge system is a promising candidate for a ferromagnetic system leaving unaffected the semiconductor surface at atomic level.

The next step was to investigate in cross section the eventual formation of identifiable structures. Figure 4.6 presents a cross-sectional HRTEM image, where the formation of agglomerates of a few nm dimension was identified. The Fourier transform of these selected areas (the equivalent of selected

area electron diffraction) allowed one to identify spots corresponding to the hexagonal close packed Mn_5Ge_3 structure. The interplanar spacings of the reciprocal lattice points indexed in Fig. 4.6(b) are 6.20, 5.08 and 3.90 Å, for the planes (100), (001), and (101), respectively. These values are in a very good agreement with the corresponding theoretical distances for the Mn_5Ge_3 compound 6.22, 5.05 and 3.92 Å, respectively, with unit-cell parameters: $a = b = 7.18$ Å and $c = 5.05$ Å [53].

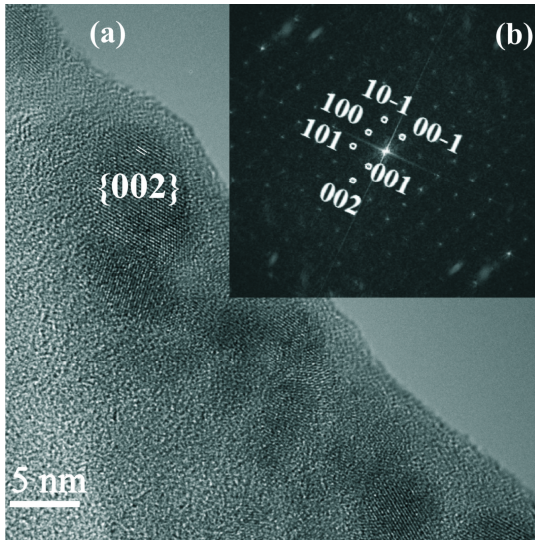


FIGURE 4.6

(a) Cross section HREM image of an area of MBE MnGe layer deposited at 350 °C; (b) the associated FFT pattern showing the presence of Mn_5Ge_3 (electron beam direction [010]). Adapted from Ref. [52]

Therefore, up to now we obtained the information that Mn diffuses inside the Ge(001) wafer and forms Mn_5Ge_3 and, possibly also $\text{Mn}_8\text{Ge}_{11}$ structures with a few nm lateral size [52]. The next question regards whether all manganese diffused into Ge(001) is involved in the formation of these nanoparticles or just a part of it. We note here that extended X-ray absorption fine structure (EXAFS) measurement at the Mn K-edge on samples grown at temperatures starting with 250 °C evidenced mainly 6 Ge neighbors for each Mn atom. EXAFS was a technique analyzing a large area of the samples, therefore this result represents an average. If the majority of Mn atoms were in Mn_5Ge_3 or $\text{Mn}_8\text{Ge}_{11}$ structures of 4-7 nm lateral size, Mn-Mn neighboring should have been easily detected. It is therefore questionable whether in some parts of the sample a truly diluted magnetic semiconductor is formed, with Mn embedded into germanium, and not just the known Mn-Ge aggregates of various stoichiometries. This will be addressed by X-ray photoelectron spectroscopy (XPS) and by magnetic measurements in the following paragraphs.

Composition (XPS)

Figure 4.7 presents XPS measurements of the Mn 2p, Ge 2p and Ge 3d core levels. An extended analysis of these data, with constant referencing to the existing literature, is available in Ref. [52]; in the following we will outline the main results.

The Ge spectra (both 3d and 2p) are characterized, upon Mn deposition, by a main photoemission line, together with a smaller component shifted by about 0.64 eV (Ge 3d) and 1.15 eV (Ge 2p) towards

higher binding energies. By comparison with the case of clean Ge(001) (2 x 1), an immediate attribution of this component is that it belongs to the observed Ge dimers at the surface, according to the LEED patterns and to the STM images. Therefore, if Ge has reacted with Mn, the formed compound has a quite close binding energy to the Ge atoms from Ge(001) single crystals.

The Mn 2p spectrum (Figure 4.7(c)) was reasonably simulated with three spin-orbit split doublets only. There are two narrow lines with low binding energies (638.50 and 639.24 eV for the $2p_{3/2}$ component), and one broader line with higher binding energies (640.61 eV). This last component was attributed in the past as being a satellite of atomic origin [54], whereas in Ref. [52] it was attributed to the formation of Mn_5Ge_3 . Anyway, without entering too much into details, there are at least two kind of manganese atoms (from the point of view of their chemical states), whereas the Ge chemical state seems to be unaffected by manganese deposition. Therefore, there are good chances that some other Mn containing structure is formed, apart from the observed Mn_5Ge_3 (and $Mn_{11}Ge_8$) clusters by HRTEM. Last but not least, band bending effects could eventually be taken into account. The Ge work function is 5.0 eV, whereas the Mn work function is 4.1 eV [55]. Therefore, for a sharp Mn-Ge interface, a maximum band bending of 0.9 eV towards higher binding energies is expected to occur [55-57]. The energy difference between the two 'sharp' components of Mn 2p is 0.74 eV, therefore one may also attribute the higher binding energy component to surface manganese, subject to the band bending downwards, as expected from a Schottky interface between a semiconductor and a metal with lower work function. Similar shifts are presented also by the Ge spectra. Thus, one may also formulate the hypothesis of chemically homogenous material formed, with a single chemical state for both manganese and germanium.

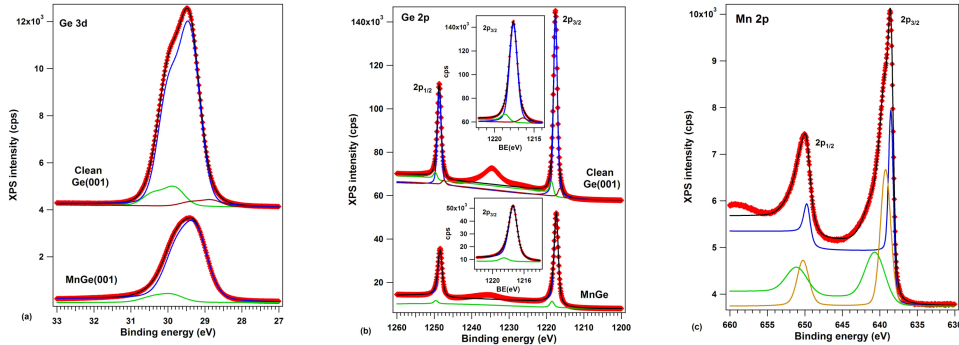


FIGURE 4.7

X-ray photoelectron spectroscopy (XPS) results: **(a)** Ge 3d core levels; **(b)** Ge 2p core levels; **(c)** Mn 2p core levels. For **(a)** and **(b)**, the spectra obtained on a clean Ge(001) (2x1) are also represented. All spectra are fitted by using Voigt doublets and integral inelastic backgrounds (see the Experimental section for details). Inserts in **(b)** are detailed regions of the Ge $2p_{3/2}$ core level. Adapted from Ref. [52]

Magnetic properties (SQUID)

It is therefore crucial to test the magnetic properties of the Mn-Ge system. In Ref. [52], magneto-optical Kerr effect measurements are presented, showing a small, though distinguishable, hysteresis loop. Another unpublished series of experiments yielded the dependence of the MOKE signals with the substrate temperature during Mn deposition: no hysteresis was observed for deposition temperatures below 250 °C, whereas the EXAFS signals for such samples exhibited a large majority of metal manganese (Mn surrounded by 12-13 other Mn atoms). The MOKE signal was analyzed, by assuming

that the majority of the signal is presented by a superparamagnetic component (i.e. a Brillouin function, equation (4) was used), and the magnetic moment derived for this component exceeded 10^4 Bohr magnetons. This would correspond to the formation of some nanoparticles with a lateral size of about 3 nm, similar to that observed by HRTEM. Therefore, an attempt of assignment was made that the superparamagnetic component belongs to the Mn_5Ge_3 ($Mn_{11}Ge_8$) clusters, whereas the remaining ferromagnetic component has another origin, possibly Mn diluted into Ge(001), therefore a diluted magnetic Mn-Ge semiconductor may be formed in a quite simple way by evaporating Mn on Ge(001) held at high temperature (solid state epitaxy [40]).

In view of all theoretical considerations developed in the first part of this Chapter, the presence or absence of a DMS-like phase may be investigated in deeper detail. Figure 4.8 presents thermomagnetic curves $M(T)$ measured by SQUID. The fact that a superparamagnetic phase is present in the film is immediately visible from the zero field cooled - field cooled (ZFC-FC) curves. As expected from superparamagnetism, the magnetization of the ZFC is low at low temperatures, increases with increasing T and reaches a plateau, which probably is obtained from separate maxima corresponding to the release of magnetization direction ('unblocking') in nanoparticles of various sizes (see § 2.2.e for more details).

But a more surprising result from Figure 4.8 is the occurrence of a peak even in the FC branch. Normally, when cooling an ensemble of ferromagnetic + superparamagnetic phases in applied field, the effective magnetization of both phases should just increase with temperature. This may be well simulated also by using the formula (9) from the first Section.

The peak in the FC curve may have two explanations: (a) a spin glass like state, see § 2.2.f; (b) the fact that the exchange integral depends on temperature and, eventually, has a peak at a given temperature or increases at higher temperatures; in the latter case, a competition between a stronger exchange integral at higher temperatures and an increased thermal disorder could eventually yield a peak. Exchange integrals varying with temperatures are a sign of indirect exchange intermediated by carriers in the semiconductor, whose concentration is clearly varying by orders of magnitudes with the temperature.

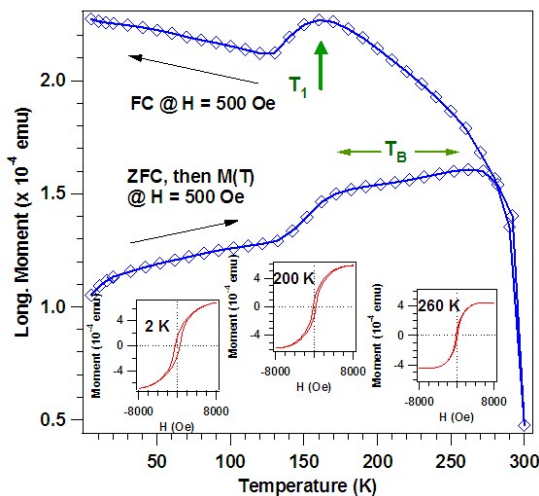


FIGURE 4.8

Superconducting quantum interference device (SQUID) measurement of the Mn-Ge(001) sample obtained by deposition of 100 nm Mn on Ge(001) held at 350 °C. The main graph with blue symbols and lines represent zero field cooled - field cooled magnetization measurements (see text for details). The inserts represent magnetisation hysteresis measurements at the specified temperatures. Adapted from Ref. [52]

Attempts to simulate the FC curve by using the Trachenko model [25] were not successful ($M \sim A + bT^2$ at low T , $M \sim C/T$ at high T). The simulation by using various theories for DMS is more complicated and will be detailed below. For the beginning, we found simpler to extract the coercitive fields from the hysteresis curves recorded at various temperatures and to simulate them by using equation (8.2), by using various models for the parameters a and b : $b = \mu_0 \mu_r n \mu_{\max}^2 / k_B T$ and a is described by equations (50-51). The results are represented in Figure 4.9.

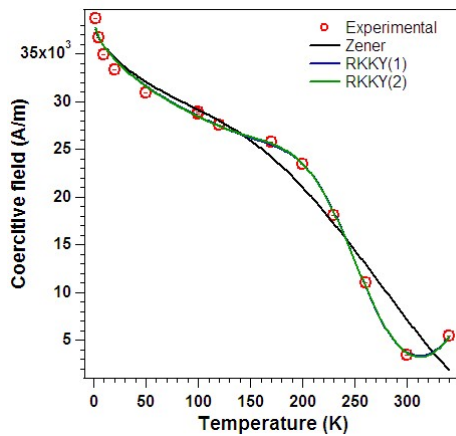


FIGURE 4.9

Dependence of the coercitive field with temperature, together with fits using formulas (8.2), (50) and (51) for Zener and for the two models of RKKY interactions, respectively.

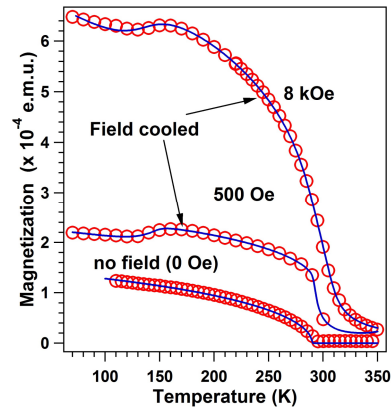


FIGURE 4.10

Simulations of the thermo-magnetization curves by using a superposition of ferromagnetic components, one with 'normal' exchange and one with RKKY interaction.

Attempts to use a 'normal' ferromagnetic phase (with both a and $b \sim 1/T$) were not successful to simulate the modulation superimposed on the constant decrease of the coercitive field with the temperature. The Zener model, equation (50), could yield some modulation, but the result of this simulation is of far lower quality than that of the simulation by using both RKKY models. Note that we assumed donor conduction in Ge(001), but all results may be valid also for acceptors, with the straightforward replacements, according to equations (49). The extracted parameters from the fit are given in Table 4.1.

One may remark that it is hard to derive values for some interesting physical quantities (e.g. the average atomic spin S , the relative permeability μ_r , or the value of various energies involved in the models), since most fitting parameters yield combinations of these quantities. The fact that the RKKY model works fine may be tested from the value of $(E_c - E_D)$, which yields about 0.18-0.22 eV, slightly lower than the Ge bandgap (0.6 eV). Also, a ferromagnetic phase coexists with the RKKY phase, with $\eta |J_{ad}| S^2 \sim 0.18$ eV. By assuming $S \sim 1$, this ferromagnetic phase would have a Curie temperature of about 300-350 K and indeed this is what one observed in the thermo-magnetization curves (Figures 4.8 and 4.10).

Coming back to the DMS-RKKY phase, it is to be noted that the obtained density of dopants largely exceeds that of the spins, therefore a majority of dopants of other nature (e.g. defects) are present in the semiconductor, apart for the manganese atoms. There are also charge carriers of almost constant concentration n_0 , most probably some parts of the sample exhibit metallic behavior. The concentration of these 'intrinsic' donors is on the same order of magnitude as that of spins n_s , therefore most

probably these carriers are produced by the manganese atoms. Also, the parameter b , which is combination of the permeability of the material and of the spin yields values of 0.13-0.14. From the significance of this parameter listed in Table 4.1 it appears that clearly one has to introduce a relative permeability μ_r of almost 10^5 .

TABLE 4.1

Interpretation and values of fitting parameters of the coercitive field dependence on temperature $H_c(T)$ from Figure 4.9 and of the thermo-magnetization curves $M(T)$ from Figure 4.10

Model Parameter	Zener	RKKY(1)	RKKY(2)
K_0 , signif.	$\frac{J_{cd}^2 g_c(\epsilon_F) S_d^2}{k_B} \left(\frac{n_d}{n_c}\right)$	$\frac{ \Delta ^2 m^* n_s^{4/3} S^2}{2h^2 k_B}$	$\frac{\eta \Delta ^2 m^* n_s^{4/3} S^2}{8\pi h^2 k_B}$
K_0 , approx. (K)	$1.16 \times 10^4 \frac{J_{cd}^2 g_c(\epsilon_F)}{1 \text{ eV}} \times S_d^2 \left(\frac{n_d}{n_c}\right)$	$0.356 \left(\frac{ \Delta }{1 \text{ Ryd.} \times \text{\AA}^3}\right)^2 S^2 \left(\frac{m^*}{m_e}\right) \times \left(\frac{n_s}{10^{27} \text{ m}^{-3}}\right)^{4/3}$	$0.0283 \left(\frac{ \Delta }{1 \text{ Ryd.} \times \text{\AA}^3}\right)^2 S^2 \times \left(\frac{m^*}{m_e}\right) \eta \left(\frac{n_s}{10^{27} \text{ m}^{-3}}\right)^{4/3}$
K_0 (K)	649	1772	225
$2N_D/n_s$	-	4251	1349
$8N_D/N_c$	105	2047	289
$\frac{E_c - E_D}{k_B}$ (K)	0.9	2487	2101
n_0/n_s	-	0.377	0.880
$\frac{2\eta J_{dd} S^2}{k_B}$ (K)	5916	3821	4137
$\frac{2\mu_0 \mu_r \mu_B S}{k_B} = 1.69 \times 10^{-6} \mu_r S$ (m·K/A) from $H_c(T)$	0.172	0.141	0.139
$\frac{2\mu_0 \mu_r \mu_B S}{k_B} = 1.69 \times 10^{-6} \mu_r S$ (m·K/A) from $M(T)$			0.711 (500 Oe) 0.735 (8 000 Oe)
$\frac{2\mu_0 \mu_r \mu_B S_{ferro}}{k_B} = 1.69 \times 10^{-6} \mu_r S_{ferro}$ (m·K/A) from $M(T)$			1.29×10^{-5} (500 Oe) 3.11×10^{-6} (8 000 Oe)
M_{ferro} / M_{DMS}			1.20 (500 Oe) 3.05 (8 000 Oe)
$\frac{2\epsilon_u}{k_B}$ (K)			874 (500 Oe) 912 (8 000 Oe)

Note also the high similarity obtained within both RKKY models used; therefore, at this level it is hard to decide which is the most appropriate.

The thermo-magnetization curves $M(T)$ were also fitted by using the $m(h)$ formula given by equation (9); the results are represented in Figure 4.10. In this case, the simulation needed to introduce a

ferromagnetic phase, whose saturation magnetization (as fitting parameter) increases with the applied field, according to Table 4.1. In view of the comments of Ref. [52], we could eventually infer that this is, in fact, superparamagnetic and might be connected to the Mn-Ge clusters observed by HRTEM; but the puzzle is that the product $\mu_r S$ is close to unity for this phase. Also, in zero applied field, this is the only phase that remains in the simulation. In fact, it was quite astonishing that, when ending the simulation of the 500 Oe case, just by setting both (bh) parameters to zero and the overall magnetization of the DMS-RKKY phase also to zero, one obtains a curve fairly close to the experimental $M(T)$ for zero applied field. Thus, one has to reconsider the value of the spin for the RKKY phase, the introduction of the relative magnetic permeability, and also its nature.

Therefore, it is the *spin* of the DMS RKKY phase which has a high value (about 83,000) in the $H_c(T)$ dependence; this corresponds to aggregates formed (approximately) by cubes with about 35 atoms on each edge, by assuming that the individual atomic spins are $S_0 = 2$. These aggregates are close to the observed Mn_5Ge_3 clusters, therefore, in addition to Ref. [52], we may affirm here that these aggregates are superparamagnetic and their mutual interaction is RKKY. Such behaviour were to be expected from very first principles from the HRTEM image; however, RKKY coupling between individual superparamagnetic nanoparticles is still a novelty and first sound reports just start to appear in literature, see. e.g. Ref. [58]. The term 'superparamagnetic' is maybe not that appropriate to describe this phase, since we have seen that it presents a coercitive field and exchange interaction between nanoparticles; but, at the same time, its contribution vanishes in the $M(T)$ curve. This may be also connected to the observation time and to the magnetic history: when just the demagnetized sample is cooled down in zero applied field, this phase does not manifest a net magnetization; when the sample, even at lower temperatures, experiences higher magnetic fields, this induces the re-orientation of the magnetic moments and stimulates the apparition of the RKKY interaction, within the observation time. The remaining, majoritary (from the magnetic point of view) component of ferromagnetic nature still needs to be explained. It may correspond to a diluted magnetic state where the magnetic ordering is characterized by nearly constant exchange integrals with temperature. Eventually, this may also correspond to a metallic character of this phase. A further support for the hypothesis of a metallic phase comes indirectly also from the analysis of an eventual band bending effect in the XPS data. Though not directly observed by our HRTEM measurements, the formation of nanocolumns, as reported in Ref. [44], cannot be precluded.

The reader may ask also why this ferromagnetic H_c phase was not needed in the simulations of $H_c(T)$ (Figure 4.9). In fact, the overall dependence of the coercitive field in the presence of two phases with different coercivities is difficult to be estimated (in any case, it is not just the sum of the two coercitive fields). One may suppose, for instance, that the coercitive field of the ferromagnetic phase is considerably lower than that of the DMS-RKKY one; for instance, it may be shown that Fe deposited on Si(001) has a quite low coercitive field, about 0.7 Oe [48], whereas pure Fe has a coercitivity of about 1 Oe [59]. Therefore, the main detected coercitivity is that of the DMS-RKKY phase.

Conclusions

This Chapter re-analyzes from very basic grounds the basic mechanisms responsible for ferromagnetism, by dividing them into direct exchange (Heisenberg and Stoner) and indirect exchange (Zener and RKKY). In view of the data that are offered as a support for practising the newly derived formula, the basic aspects of superparamagnetism and of the spin glass state were also briefly reviewed. The 'theoretical' section offers approximate formulas which one may use for simulating all kind of dependencies from the general form of magnetization dependence on applied field and

temperature $M(H, T)$: the dependence on temperature of the coercitive field $H_c(T)$, of the remanent magnetization $M_r(T)$, or the hysteresis curves $M(H)$. The reader is encouraged to implement these formulas (8-9) into any simulation program and to derive e.g. the departure from the Curie-Weiss law in ferromagnets near T_c , or various hysteresis or thermomagnetic curves. The aim of this methodology was to offer a modality to trace the way from the experimental data back to the relevant parameters and to derive mechanisms responsible for magnetization (a kind of 'inverse problem').

An example of this data regression on a somehow complicated, though quite actual system: manganese-germanium, is presented in the second part of the Chapter. Data from measurements other than magnetic are presented in order to characterize as much as possible by other means the proposed system. Through the data regression, we were able to simulate in a satisfactory way the dependencies $H_c(T)$ and $M(T)$ (field cooled). The novelty of this study is that it pointed out not only on the existence of interacting superparamagnetic nanoparticles, but also on the fact that these nanoparticles interact mutually by the RKKY mechanism. This phase coexists with a strong ferromagnetic phase, described by exchange integrals which do not depend on temperature, at least in the temperature range investigated.

As a whole, the manganese-germanium system presented here exhibits unusual magnetic properties and, in our opinion, the most important facts is that it provides ferromagnetism near room temperature, and that the behavior of the magnetization with temperature is non-monotonous, being described by indirect exchange mechanisms, opening possibilities for some practical applications which may lead to an interplay between magnetism with other physical quantities *via* the density of the charge carriers in germanium.

Acknowledgements

We acknowledge valuable help from Dr. Florin Vasiliu with HRTEM investigations and from Dr. Victor Kuncser with the SQUID measurements. This work was funded by the Romanian national funding agency through the Contracts PN2-Partnerships Nos. 152/2011 and 128/2011 and by the NIMP Kernel Programme 45N/2009.

References

1. Jiles D. Introduction to Magnetism and Magnetic Materials. Boca Raton: Taylor & Francis; 1998, p. 299.
2. Cohen A. A Padé approximant to the inverse Langevin function. *Rheologica Acta* 1991; 30: 270-273.
3. Stoner EC, Wohlfarth, EP. A mechanism of magnetic hysteresis in heterogeneous alloys. *Philosophical Transactions of the Royal Society A: Physical, Mathematical and Engineering Sciences* 1948; 240 (826): 599–642.
4. Callen E, Liu YJ, Cullen JR, Initial magnetization, remanence, and coercivity of the random anisotropy amorphous ferromagnet. *Physical Review B* 1977; 16(1): 263-270.
5. Sommerfeld A, Bethe H. *Elektronentheorie der Metalle*. Handbuch der Physik, Volume 24/2, pp 333-622 Springer, Berlin, 1933.
6. Morán S, Ederer C, Fähnle M. Ab initio electron theory for magnetism in Fe: Pressure dependence of spin-wave energies, exchange parameters, and Curie temperature. *Physical Review B* 2003; 67(1): 012407.
7. Mokrousov Y, Bihlmayer G, Blügel S, Heinze S. Magnetic order and exchange interactions in monoatomic 3d transition-metal chains. *Physical Review B* 2007; 75(10): 104413.
8. Nolting W, Ramakanth A. *Quantum Theory of Magnetism*. Berlin: Springer; 2009, p. 393.
9. Teodorescu CM, Lungu GA. Band ferromagnetism in systems of variable dimensionality. *Journal of Optoelectronics and Advanced Materials* 2008; 10(11): 3058-3068.
10. Lungu GA, Teodorescu CM. Band ferromagnetism in systems of variable dimensionality II: the two-dimensional finite temperature case 2009; 11(4): 369-379.
11. Lungu GA, Apostol NG, Morariu M, Teodorescu CM. Band ferromagnetism in systems with linear density of states. *Digest Journal of Nanomaterials and Biostructures* 2012; 7(4): 1615-1626.
12. Albrecht M, Maret M, Köhler J, Gilles B, Poinso R, Hazemann JL, Tonnerre JM, Teodorescu C, Bucher E. Ferromagnetic hcp chromium in Cr/Ru(0001) superlattices. *Physical Review Letters* 2000; 85(25): 5344-5347.
13. Albrecht M, Maret M, Köhler J, Gilles B, Poinso R, Hazemann JL, Tonnerre JM, Teodorescu C, Bucher E. Structural and magnetic properties of Cr in Cr/Ru(0001) multilayers. *Physical Review B* 2002; 66(20): 205410(1-9).
14. Huttel Y, van der Laan G, Teodorescu CM, Bencok P, Dhesi SS. Magnetic V embedded in copper evidenced by x-ray magnetic circular dichroism. *Physical Review B* 2003; 67(5): 052408(1-4).
15. Stoner EC, Collective electron ferromagnetism. *Proceedings of the Royal Society of London* 1938; 165: 372.
16. Kobayashi M, Kai T, Takano N, Shiiki K, The possibility of ferromagnetic BCC ruthenium. *Journal of Physics: Condensed Matter* 1995; 7(9): 1835-1842
17. Zener C, Interaction between d shells in the transition metals. *Physical Review* 1951; 81(4): 440.
18. Anderson PW, Antiferromagnetism. The theory of superexchange interaction. *Physical Review* 1950; 79(2): 350.
19. Néel, L, Théorie du traînage magnétique des ferromagnétiques en grains fins avec applications aux terres cuites. *Annales de Géophysique* 1949; 5: 99-136.

20. Pana O, Teodorescu CM, Chauvet O, Payen C, Macovei D, Turcu R, Soran ML, Aldea N, Barbu N, Structure, morphology and magnetism of Fe-Au core-shell nanoparticles. *Surface Science* 2007; 601: 4352-4357.
21. Brown WF, Thermal fluctuations of a single-domain particle. *Physical Review* 1963; 130(5): 1677-1686.
22. Ford PJ, Spin glasses. *Contemporary Physics* 1982; 23(2): 141-168.
23. Edwards SF, Anderson PW, Theory of spin glasses. *Journal of Physics F: Metal Physics* 1975; 5(5), 965-974.
24. Sherrington D, Kirkpatrick S, Solvable model of a spin glass. *Physical Review Letters* 1975; 35(26): 1792-1796.
25. Trachenko K, Understanding the spin glass transition as a dynamic phenomenon, *Journal of Physics: Condensed Matter* 2011; 23: 366003.
26. Ruderman M.A., Kittel C, Indirect exchange coupling of nuclear magnetic moments by conduction electrons, *Physical Review* 1954; 96(1): 99-102
27. Kasuya T, A theory of metallic ferro- and antiferromagnetism on Zener's Model. *Progress of Theoretical Physics* 1956; 16(1), 45-57
28. Yosida K, Magnetic properties of Cu-Mn alloys, *Physical Review* 1957; 106(5): 893-898.
29. Kittel C, *Introduction to Solid State Physics*. 8th Edition. New York: Wiley; 2005, p. 167.
30. Bransden BH, Joachain CJ, *Physics of Atoms and Molecules*. London: Longman; 1990, p. 109.
31. Sze SM, *Physics of Semiconducting Devices*. Hoboken: Wiley; 1981, p. 25
32. Park YD, Hanbicki AT, Erwin SC, Hellberg CS, Sullivan JM, Mattson JE, Ambrose TF, Wilson A, Spanos G, Jonker BT. A Group-IV Ferromagnetic Semiconductor: Mn_xGe_{1-x} . *Science* 2002; 295(5555): 651-654.
33. Tsui F, He L, Ma L, Tkachuk A, Chu YS, Nakajima K, Chikyow T. Novel Germanium-Based Magnetic Semiconductors. *Physical Review Letters* 2003; 91(17): 177203(1-4).
34. Huttel Y, Teodorescu CM, Bertran F, Krill G. Experimental evidence of long range magnetic order in the $c(2 \times 2)$ MnCu(100) surface alloy. *Physical Review B* 2001; 64(9): 094405(1-4).
35. Sangaletti L, Ghidoni D, Pagliara S, Goldoni A, Morgante A, Floreano L, Cossaro A, Mozzati MC, Azzoni CB. Electronic properties of the ordered metallic Mn:Ge(111) interface. *Physical Review B* 2005; 72(3); 035434(1-6).
36. Zheng C, Zhang Z, van Benthem K, Chisholm MF, Weitering HH. Optimal Doping Control of Magnetic Semiconductors via Subsurfactant Epitaxy. *Physical Review Letters* 2008; 100(6): 066101(1-4).
37. Hansen M, Anderko K. *Constitution of Binary Alloys*. New York: McGraw-Hill; 1958, p. 766.
38. Zeng C, Erwin SC, Feldman LC, Li AP, Jin R, Song Y, Thompson JR, Weitering HH. Epitaxial ferromagnetic Mn_5Ge_3 on Ge(111). *Applied Physics Letters* 2003; 83(24): 5002-5004.
39. Kang JS, Kim G, Wi SC, Lee SS, Choi S, Cho S, Han SW, Kim KH, Song HJ, Shin HJ, Sekiyama A, Kasai S, Suga S, Min BI. Spatial Chemical Inhomogeneity and Local Electronic Structure of Mn-Doped Ge Ferromagnetic Semiconductors. *Physical Review Letters* 2005; 94(14): 147202(1-4).
40. De Padova P, Ayoub J-P, Berbezier I, Perfetti P, Quaresima C, Testa AM, Fiorani D, Olivieri B, Mariot J-M, Taleb-Ibrahimi A, Richter MC, Heckmann O, Hricovini K. $Mn_{0.06}Ge_{0.94}$ diluted magnetic semiconductor epitaxially grown on Ge(001): Influence of Mn_5Ge_3 nanoscopic clusters on the electronic and magnetic properties. *Physical Review B* 2008; 77(4): 045203(1-7).
41. Zeng C, Zhu W, Erwin SC, Zhang Z, Weitering HH. Initial stages of Mn adsorption on Ge(111). *Physical Review B* 2004; 70(20): 205340(1-8).

42. Ahlers S, Stone PR, Sircar N, Arenholz E, Dubon OD, Bougeard, D. Comparison of the magnetic properties of GeMn thin films through Mn L-edge x-ray absorption. *Applied Physics Letters* 2009; 95(15): 151911(1-3).
43. Ahlers S, Bougeard D, Sircar N, Abstreiter G, Trampert A, Opel M, Gross R. Magnetic and structural properties of $\text{Ge}_x\text{Mn}_{1-x}$ films: Precipitation of intermetallic nanomagnets. *Physical Review B* 2006; 74(21): 214411(1-8).
44. Jamet M, Barski A, Devillers T, Poydenot V, Dujardin R, Bayle-Guillemaud P, Rothman J, Bellet-Amalric E, Marty A, Cibert J, Mattana R, Tatarenko S. High-Curie-temperature ferromagnetism in self-organized $\text{Ge}_{1-x}\text{Mn}_x$ nanocolumns. *Nature Materials* 2006; 5: 653-659.
45. Mouton I, Lardé R, Talbot E, Cadel E, Genevois C, Blavette D, Baltz V, Prestat E, Bayle-Guillemaud P, Barski A, Jamet M. Composition and morphology of self-organized Mn-rich nanocolumns embedded in Ge: Correlation with the magnetic properties. *Journal of Applied Physics* 2012; 112(11): 113918(1-7).
46. Olive-Mendez S, Spiesser A, Míchez LA, Le Thanh V, Glachant A, Derrien J, Devillers T, Barski A, Jamet M. Epitaxial growth of $\text{Mn}_5\text{Ge}_3/\text{Ge}(111)$ heterostructures for spin injection. *Thin Solid Films* 2008; 517: 191-196.
47. Lungu GA, Apostol NG, Ștoflea LE, Costescu RM, Popescu DG, Teodorescu CM. Room temperature ferromagnetic, anisotropic, germanium rich $\text{FeGe}(001)$ alloys. *Materials* 2013; 6: 612-625.
48. Gheorghe NG, Husanu MA, Lungu GA, Costescu RM, Macovei D, Teodorescu CM. Atomic structure and reactivity of ferromagnetic Fe deposited on $\text{Si}(001)$. *Journal of Materials Science* 2012; 47: 1614-1620.
49. Gheorghe NG, Husanu MA, Lungu GA, Costescu RM, Macovei D, Popescu DG, Teodorescu CM. Reactivity, magnetism and local atomic structure in ferromagnetic Fe layers deposited on $\text{Si}(001)$. *Digest Journal of Nanomaterials and Biostructures* 2012; 7(1): 373-384.
50. Costescu RM, Gheorghe NG, Husanu MA, Lungu GA, Macovei D, Pintilie I, Popescu DG, Teodorescu CM. Epitaxial ferromagnetic samarium and samarium silicide synthesized on $\text{Si}(001)$. *Journal of Materials Science* 2012; 47: 7225-7234.
51. Gheorghe NG, Lungu GA, Husanu MA, Costescu RM, Macovei D, Teodorescu CM. Structure, reactivity, electronic configuration and magnetism of samarium atomic layers deposited on $\text{Si}(001)$ by molecular beam epitaxy. *Applied Surface Science* 2013; 267: 106-111.
52. Lungu GA, Ștoflea LE, Tănase LC, Bucur IC, Răduțoiu N, Vasiliu F, Mercioniu I, Kuncser V, Teodorescu CM, Room temperature ferromagnetic $\text{Mn:Ge}(001)$. *Materials* 2014; 6: 106-129.
53. Passacantando M, Ottaviano L, D'Orazio F, Lucari F, De Biase M, Impellizzeri G, Priolo F. Growth of ferromagnetic nanoparticles in a diluted magnetic semiconductor obtained by Mn^+ implantation on Ge single crystals. *Physical Review B* 2006; 73(19): 195207(1-5).
54. Sangaletti L, Drera G, Magnano E, Bondino F, Cepek C, Sepe A, Goldoni A. Atomic approach to core-level spectroscopy of delocalized systems: Case of ferromagnetic metallic Mn_5Ge_3 . *Physical Review B* 2010; 81(8): 085204(1-6).
55. Apostol NG, Ștoflea LE, Lungu GA, Chirilă C, Trupină L, Negrea RF, Ghica C, Pintilie L, Teodorescu CM. Charge transfer and band bending at $\text{Au/Pb}(\text{Zr,Ti})\text{O}_3$ interfaces investigated by photoelectron spectroscopy. *Applies Surface Science* 2013; 273: 415-425.
56. Apostol NG, Ștoflea LE, Lungu GA, Tănase LC, Chirilă C, Frunză L, Pintilie L, Teodorescu CM. Band bending in $\text{Au/Pb}(\text{Zr,Ti})\text{O}_3$ investigated by X-ray photoelectron spectroscopy: dependence on the initial state of the film. *Thin Solid Films* 2013; 545: 13-21.

57. Apostol NG, Ștoflea LE, Lungu GA, Tache CA, Pintilie L, Teodorescu CM. Band bending at free Pb(Zr,Ti)O₃ surfaces analyzed by X-ray photoelectron spectroscopy. *Materials Science and Engineering B* 2013; 178: 1317-1322.
58. Zheng WW, Strouse GF. Involvement of Carriers in the Size-Dependent Magnetic Exchange for Mn: CdSe Quantum Dots. *Journal of the American Chemical Society* 2011; 133: 7482–7489.
59. Lide D (Editor-in-Chief). *Handbook of Chemistry and Physics*, 75th Edition. Boca Raton: CRC Press; 1994, p. 12-112.